INVESTIGATING THE PHYSIOLOGICAL FUNCTION OF A *STAPHYLOCOCCUS AUREUS* NTN-HYDROLASE

by

Brigid Conroy

B.Sc., Queen's University, 2016

A THESIS SUBMITTED IN PARTIAL FULFILLMENT OF

THE REQUIREMENTS FOR THE DEGREE OF

MASTER OF SCIENCE

in

THE FACULTY OF GRADUATE AND POSTDOCTORAL STUDIES

(Microbiology and Immunology)

THE UNIVERSITY OF BRITISH COLUMBIA

(Vancouver)

June 2019

The following individuals certify that they have read, and recommend to the Faculty of Graduate and Postdoctoral Studies for acceptance, a thesis/dissertation entitled:

INVESTIGATING THE PHYSIOLOGICAL FUNCTION OF A *STAPHYLOCOCCUS AUREUS* NTN-HYDROLASE

submitted by Brigid Conroy in partial fulfillment of the requirements for

the degree of Master of Science

in Microbiology and Immunology

Examining Committee:

Dr. Michael Murphy, Microbiology and Immunology
Supervisor

Dr. Lawrence McIntosh, Biochemistry and Molecular Biology
Supervisory Committee Member

Dr. John Smit, Microbiology and Immunology
Additional Examiner

Additional Supervisory Committee Members:

Dr. Rachel Fernandez, Microbiology and Immunology
Supervisory Committee Member

Abstract

The N-terminal nucleophile (Ntn)-hydrolase structural superfamily consists of several classes of enzymes, including the penicillin V acylases (PVAs), bile salt hydrolases, and *N*-acylhomoserine lactone (AHL) acylases. The PVAs use an N-terminal cysteine residue to hydrolyze the amide bond in penicillin V and are most closely related to the bile salt hydrolases. PVAs are encoded by many environmental and pathogenic bacteria and are of great importance in the pharmaceutical industry because the product of penicillin V hydrolysis is used in the production of semi-synthetic antibiotics. Despite their industrial value, the physiological function of the PVAs remains unknown. The opportunistic human pathogen *Staphylococcus aureus* encodes an Ntn-hydrolase (gene locus SAUSA300_0269). Several potential substrates of SAUSA300_0269 were tested and it was demonstrated to hydrolyze penicillin V but show no activity towards the bile salt glycocholic acid. Based on the observed activity, SAUSA300_0269 was renamed to *Sa*PVA. This enzyme also hydrolyzed several AHLs, which are quorum sensing molecules used by Gram-negative bacteria. *Sa*PVA is the first example of a PVA from a Gram-positive bacterium that cross-reacts with AHLs. The enzyme displayed a preference for unsubstituted AHLs with an acyl chain of six or more carbons. Growth experiments did not support a role for *Sa*PVA in protection of *S. aureus* against the toxicity of 3-oxo-C_{12}-HSL, an AHL produced by *Pseudomonas aeruginosa*. Two siderophores used by *S. aureus*, enterobactin and staphyloferrin A, were also tested as substrates, but *Sa*PVA did not show activity towards either molecule.

To obtain further insight into the substrates of *Sa*PVA, the crystal structure was solved to 1.9 Å resolution and compared with those of other characterized PVAs from Gram-positive and Gram-negative bacteria. Similarity in the overall structure and substrate-binding loops of PVAs

from Gram-positive bacteria suggest that these enzymes act on similar substrates. Molecular docking was used to predict the binding modes of penicillin V and various AHLs to *Sa*PVA. Docking results provided some clues about the structural features that may be present in physiological substrates of *Sa*PVA, including one or more rings, as well as an aryl group or hydrophobic acyl chain.

Lay Summary

Staphylococcus aureus is a bacterium that can cause serious infections in humans. It produces an enzyme that cleaves the antibiotic penicillin V. The enzyme family is important in the pharmaceutical industry because one product of the cleavage can be used to produce new antibiotics with improved characteristics. The function of the enzyme in the bacterium, however, is unknown. The purpose of this study was to determine what other molecules are cleaved by the enzyme to gain insight into its function. Molecules that are used by certain bacteria for communication were also cleaved by the enzyme. These molecules are toxic to *S. aureus* but the results did not support the hypothesis that the enzyme functions to protect the bacteria from their toxic effects. The structure of the enzyme and how molecules bind to its active site were also studied to inform predictions of other molecules that may be cleaved.

Preface

The work in this thesis includes contributions by fellow scientists in the Murphy lab. Dr. Meghan Verstraete and L. Daniela Morales designed the original *sapva* construct for protein expression. The *sapva* deletion strain was produced by Dr. Jason Grigg and Joshua Bray. The staphyloferrin A HPLC assay was developed and optimized in a collaborative effort between Dr. Jason Grigg, Mariko Ikehata, and Maxim Kolesnikov. All other work described in this thesis is my original, unpublished work.

This project required biohazard approval for the handling of *Escherichia coli* and *Staphylococcus aureus.* Approval was provided by the UBC Biosafety Committee, Certificate number: B17-0242.

Table of Contents

List of Tables

List of Figures

List of Abbreviations

6-APA	6-aminopenicillanic acid
AHL	*N*-acylhomoserine lactone
AI	Autoinducer
BSH	Bile salt hydrolase
CG	Cholylglycine
CLS	Canadian Light Source
DMSO	Dimethyl sulfoxide
DNA	Deoxyribonucleic acid
Fur	Ferric uptake regulator
HEPES	4-(2-hydroxyethyl)-1-piperazineethanesulfonic acid
HPLC	High performance liquid chromatography
HSL	Homoserine lactone
IPTG	Isopropyl β-D-thiogalactopyranoside
LB	Luria-Bertani
MRSA	Methicillin resistant *Staphylococcus aureus*
Ntn	N-terminal nucleophile
PCR	Polymerase chain reaction
*p*DAB	*p*-dimethylaminobenzaldehyde
PDB	Protein Data Bank
PEG	Polyethylene glycol
PVA	Penicillin V acylase

QS	Quorum sensing
QTOF	Quadrupole time of flight
RMSD	Root mean square deviation
RPMI-1640	Roswell Park Memorial Institute-1640
SA	Staphyloferrin A
SB	Staphyloferrin B
SDS-PAGE	Sodium dodecyl sulphate polyacrylamide gel electrophoresis
TCEP	Tris(2-carboxyethyl)phosphine
TSB	Tryptic soy broth

Acknowledgements

I acknowledge funding from a Canadian Graduate Scholarships – Master's award provided by the Natural Sciences and Engineering Research Council of Canada. This research was also funded by Canadian Institutes of Health Research grants held by Dr. Michael Murphy.

I would like to express my gratitude to Dr. Michael Murphy for the opportunity to conduct research in his laboratory and for his guidance and mentorship regarding both my research project and career goals. I am also grateful to my committee members, Dr. Lawrence McIntosh and Dr. Rachel Fernandez, for providing valuable feedback and advice about my research.

I would like to sincerely thank the members of the Murphy lab, past and present, for their advice, support, and kindness. To Angelé, thank you for your help in learning lab techniques and your willingness to listen when I encountered experimental difficulties. To Jason, thank you for helping me to improve my scientific writing. To Jenn, thank you for being an amazing friend and a pillar of support over the past three years.

I would also like to thank my friends and family for their support through the ups and downs of research. To Sean, thank you for your patience, understanding, and for brightening all of my days. To my mom, thank you for your unwavering emotional support, for teaching me resilience, and for always believing in me.

Chapter 1: Introduction

1.1 *Staphylococcus aureus*

1.1.1 Pathogenesis

Staphylococcus aureus is a Gram-positive opportunistic pathogen capable of causing a wide range of infections in humans (1). *S. aureus* is normally a commensal that asymptomatically colonizes the skin and mucous membranes in a proportion of the human population (2–4). The principal reservoir of *S. aureus* is the anterior nares, but it can also colonize other sites, including the underarms, groin, and gastrointestinal tract (2, 5, 6). Colonization rates vary by population, and are higher in hemodialysis and surgical patients and those with type 1 diabetes or acquired immunodeficiency syndrome (7). When the skin or mucosal barrier is breached, for example during surgery or catheter insertion, *S. aureus* can infiltrate the tissues and bloodstream (7). *S. aureus* causes infections that range from superficial, such as impetigo, to invasive and life-threatening, such as endocarditis, osteomyelitis, toxic shock syndrome, and sepsis (1, 7).

1.1.2 Antibiotic resistance

Treatment of *S. aureus* infections is complicated by the prevalence of multidrug-resistant strains. Penicillin-resistant isolates were reported shortly after the introduction of penicillin in 1944 (8, 9). This resistance was mediated by the production of a secreted β-lactamase, which destroys penicillin through hydrolysis of the four-membered lactam ring (10). Methicillin is a penicillin derivative that is insensitive to some β-lactamases due to the introduction of a bulky group that sterically hinders enzymatic attack (10). *S. aureus* isolates resistant to methicillin were first identified in 1961, less than a year after its introduction (11). Methicillin resistance is mediated by the *mecA* gene, which encodes a penicillin-binding protein (PBP2a) with low affinity for β-lactam

antibiotics (10). Until the 1990's, methicillin-resistant *S. aureus* (MRSA) almost exclusively caused infection in patients exposed to a healthcare setting (5). Community-associated MRSA strains are increasingly prevalent, however, and can cause severe disease in healthy individuals (12). In 2004, the direct healthcare costs associated with MRSA in Canada were estimated at $82 million and were projected to increase in the following years (13). Serious concern was prompted by the observation of vancomycin resistance in 2002, as this glycopeptide antibiotic is considered the drug of last resort against MRSA (14, 15).

1.2 N-terminal nucleophile-hydrolase superfamily

Brannigan *et al.* (1995) first identified the protein structural superfamily known as the N-terminal nucleophile (Ntn)-hydrolases. Ntn-hydrolases share a common αββα fold composed of two stacked antiparallel β-sheets flanked on both sides by a layer of antiparallel α-helices (Figure 1-1) (16). The catalytically-active N-terminal residue is located within one of the core β-sheets (17). The side chain of the N-terminal cysteine, serine, or threonine residue carries out a nucleophilic attack on the carbonyl group of an amide bond (17, 18). While all Ntn-hydrolases cleave an amide bond, their substrate specificities and quaternary structures vary widely (16, 18). Members of this superfamily include penicillin acylases (19), cephalosporin acylases (20), *N*-acylhomoserine lactone hydrolases (21), class II glutamine amidotransferases (22), lysosomal aspartylglucosaminidase (23), and proteasome α- and β-subunits (Figure 1-2) (24). In addition to amide bond hydrolysis, most Ntn-hydrolases carry out autocatalytic processing of the proenzyme to expose the nucleophilic residue at the N-terminus (17). Based on similarities in their overall fold, catalytic residues, and enzyme function, a common evolutionary origin has been suggested

for the Ntn-hydrolases (16, 17). Nonetheless, sequence similarity between members of this superfamily is low, suggesting significant divergence (17).

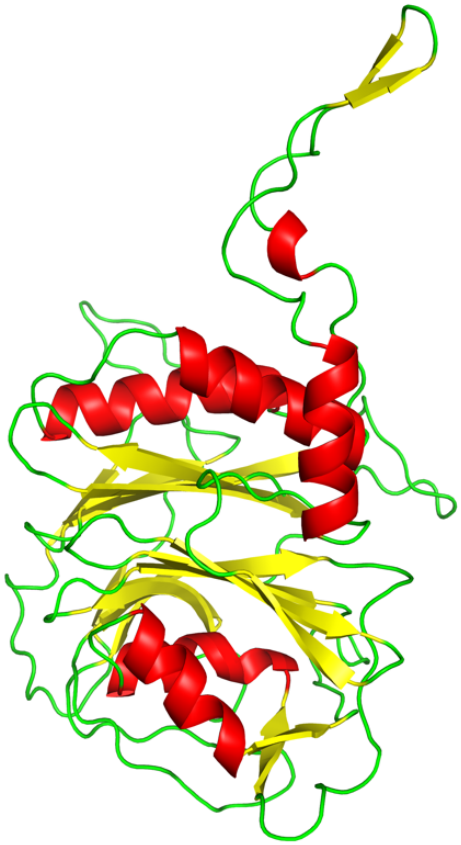

Figure 1-1. Overall fold conserved within the Ntn-hydrolase superfamily.
Cartoon representation of a protomer of penicillin V acylase from *Bacillus subtilis* (PDB ID: 2OQC), a member of the Ntn-hydrolase superfamily. Loops are coloured green, α-helices are coloured red, and β-sheets are coloured yellow. The αββα fold consists of two antiparallel β-sheets packed together with a layer of antiparallel α-helices on both sides.

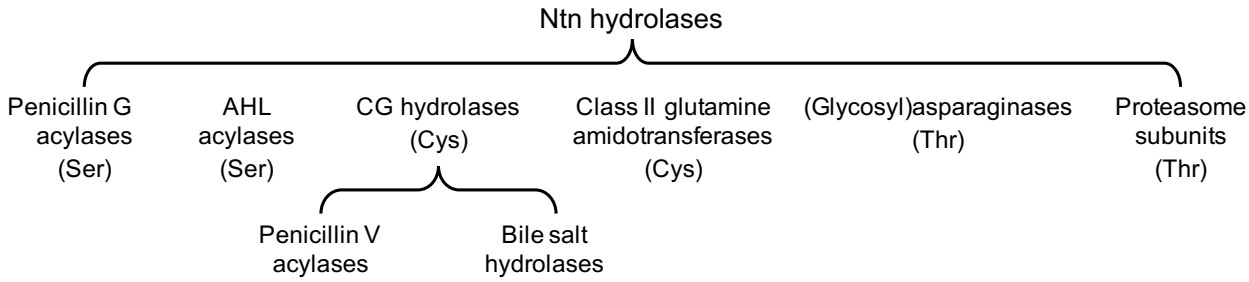

Figure 1-2. Schematic of select enzyme classes within the Ntn-hydrolase superfamily.
The Ntn-hydrolase superfamily encompasses several classes of enzymes, six of which are shown. The N-terminal nucleophilic residue used by each class of enzymes is indicated in brackets. Within the CG hydrolase family are two types of enzymes: bile salt hydrolases and penicillin V acylases.

1.3 Cholylglycine hydrolase family

1.3.1 General background

One family of enzymes within the diverse Ntn-hydrolase superfamily is the cholylglycine (CG) hydrolases (EC 3.5.1.24). The CG hydrolase family is composed of two classes of evolutionarily-related enzymes: the bile salt hydrolases (BSHs) and penicillin V acylases (PVAs; Figure 1-2) (25). All members of the CG hydrolase family use cysteine as the N-terminal nucleophilic residue and form a homotetrameric quaternary structure (25). The *S. aureus* protein of interest is encoded by the gene SAUSA300_0269 and is annotated as a CG hydrolase.

1.3.2 Bile salt hydrolases

Bile salts are cholesterol derivatives that are synthesized in the liver via conjugation of the amino acids glycine or taurine to a steroid ring moiety (26). Bile salts are secreted into the intestinal lumen and are involved in absorption of dietary lipids and endocrine signaling (27, 28). They have also been shown to limit bacterial growth in the small intestine (29–31). BSHs catalyze hydrolysis of the amino acid moiety of conjugated bile salts (Figure 1-3), to release a free primary bile acid (26). BSHs are produced mainly by gut-inhabiting bacteria (26, 32, 33) but have also been

identified in some pathogens and implicated as a virulence factor involved in pathogenesis (34, 35). BSHs are thought to protect gut bacteria from the anti-microbial activity of bile salts, thereby enhancing bacterial survival (26).

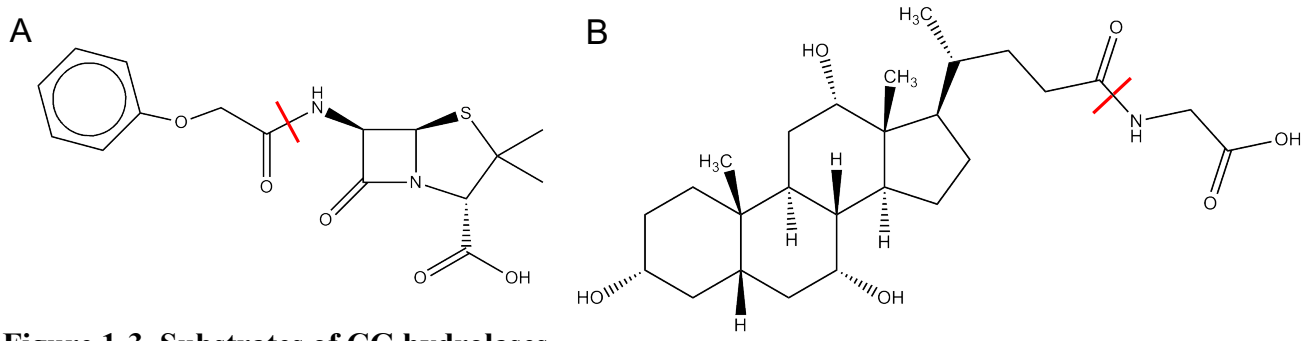

Figure 1-3. Substrates of CG hydrolases.
Structures of (A) penicillin V, and (B) glycocholic acid, a conjugated bile salt. The amide bonds hydrolyzed by bile salt hydrolases and penicillin V acylases, respectively, are indicated with a red line.

1.3.3 Penicillin V acylases

PVAs hydrolyze the linear amide bond in phenoxymethylpenicillin (penicillin V; Figure 1-3), producing 6-aminopenicillanic acid (6-APA) and phenoxyacetic acid (36). PVA enzymes are distributed among pathogenic bacteria and environmental microbes, including soil and aquatic bacteria (33). PVAs have significant value in the pharmaceutical industry because 6-APA is a precursor in the production of semi-synthetic β-lactam antibiotics (36, 37). The majority of papers in the literature on PVAs are focused on the industrial uses of these enzymes, including improvements in enzyme production and immobilization, optimization of activity by mutagenesis and protein engineering, and discovery of new enzymes (37–39). Despite the interest in their industrial applications, the physiological functions of PVAs remain unknown.

Penicillin V is unlikely to be the physiological substrate of PVA enzymes (36, 40). Several penicillin acylases exhibit substrate flexibility, acting on a wide range of molecules, and

deacylation of penicillin does not confer an evolutionary advantage (36). Cole and Sutherland (1966) determined that penicillin acylase activity was not a significant factor in the penicillin resistance observed in 148 clinical isolates of Gram-negative bacteria. Even when penicillin acylase activity was present, penicillin inactivation was due primarily to β-lactamase activity (41).

One hypothesis regarding the biological function of penicillin acylases, including PVAs, is that these enzymes are involved in scavenging phenolic compounds produced by the action of microorganisms on plant matter when the bacteria are in a non-parasitic environment (36, 40). The gene encoding the *Escherichia coli* penicillin G acylase is associated with the operon responsible for phenylacetic acid catabolism, but no such information is available for PVAs (42, 43). An alternative hypothesis is that PVAs are involved in the degradation of quorum sensing molecules. This hypothesis was prompted by observation of cross-reactivity between PVAs and another class of enzymes within the Ntn-hydrolase superfamily, the *N*-acylhomoserine lactone (AHL) acylases, which is discussed in Section 1.4.3 (44, 45). Finally, sub-inhibitory concentrations of some antibiotics have been observed to act as signaling molecules that facilitate communication between species in microbial communities (46). While this phenomenon has not been studied for β-lactam antibiotics, it is possible they mediate interspecies signaling and that PVAs play a role in this system (36).

1.3.4 Phylogenetic and binding site analyses

BSHs and PVAs cannot be reliably distinguished based on sequence similarity alone, which prompted two groups to conduct phylogenetic and binding site-similarity analyses to improve the annotation of CG hydrolases (32, 33). In phylogenetic analyses by both Lambert *et al.* (2008) and Panigrahi *et al.* (2014), the CG hydrolase sequences were distributed into two major clusters, one of which contains sequences from primarily Gram-positive bacteria and the other

from primarily Gram-negative bacteria. Experimentally-verified BSHs and PVAs are present in both clusters. Another major difference between the two clusters is the length of the sequence that precedes the catalytic cysteine (33). For the majority of sequences in cluster 1 (Gram-positive), only one methionine residue precedes the cysteine residue. This *N*-formyl methionine is usually removed by a methionyl aminopeptidase in the bacterium (33, 47–50). The longer peptide sequence that precedes the catalytic cysteine in the sequences of cluster 2 (Gram-negative) functions as a signal sequence for secretion into the periplasmic space (33). This sequence is likely autocatalytically removed, as is common amongst the Ntn-hydrolases (51). All cluster 1 sequences also contain a 13-19 amino acid "assembly motif" that contributes to the assembly and stabilization of the tetrameric quaternary structure (33). The tetramer is less thermodynamically stable for enzymes in cluster 2 due to the absence of this motif (33).

Cluster 1 is further divided into two groups, one containing BSHs and the other containing PVAs (33). The protein of interest, encoded by SAUSA300_0269, falls within cluster 1 and is annotated as a PVA. Importantly, the annotation of a CG hydrolase as a BSH or PVA indicates solely whether the enzyme activity is greater for bile salts or penicillin V. While some enzymes are solely BSHs or PVAs and have no activity towards the other substrate, some BSHs have low levels of activity towards penicillin V and vice versa (25, 33). Kumar *et al.* (2006) determined that this gradation in activity is reflected in the amino acid sequences of the enzymes, which supports the hypothesis that BSHs and PVAs diverged from a common evolutionary ancestor.

1.3.5 Catalytic mechanism

Amide bond hydrolysis by Ntn-hydrolases occurs through two consecutive half-reactions. In the first, the cysteine alpha-amino group protonates the leaving group nitrogen and, in a concerted fashion, the anionic thiolate group carries out a nucleophilic attack on the carbonyl group

of the amide bond (52). The amino leaving group is released and an acylenzyme adduct is formed. For hydrolysis of penicillin V, the leaving group is 6-APA and phenoxyacetic acid forms the enzyme adduct (53). In the second half-reaction, a water molecule participates in cleavage of the acylenzyme adduct to regenerate the enzyme (52).

The roles of several conserved residues involved in PVA activity have been inferred based on computational analysis and mutagenesis of a BSH (52). Residues Arg17 and Asp20 (numbering based on the PVA from *Bacillus sphaericus*) likely stabilize the anionic thiolate group of the catalytic cysteine and residue Asn175 likely stabilizes the transition state as part of the oxyanion hole (52). In the studied BSH, residue Asn82 also contributes to the oxyanion hole, but in PVAs, this Asn residue is replaced with a Tyr (33, 52). Finally, residue Arg228 in the studied BSH is directly involved in transition-state stabilization and, in docking studies with a PVA, the homologous residue forms a hydrogen bond with penicillin V (33, 52).

1.4 Hydrolysis of *N*-acylhomoserine lactones

1.4.1 Quorum sensing in Gram-negative bacteria

Quorum sensing (QS) is a cell-to-cell communication system that allows bacteria to coordinate their activities in response to population density through regulation of gene expression (54, 55). For example, QS systems have been implicated in regulation of virulence factor secretion (56), biofilm formation (57), antibiotic production (58), and swarming migration (59). Intercellular communication in QS systems is mediated by diffusible signaling molecules termed autoinducers (AIs) (60). AIs are secreted by bacteria and accumulate in the local environment as the bacterial population increases (61). When a threshold population density is reached, AIs interact with cognate receptor proteins in the membrane or cytoplasm (54, 61). Detection of AIs upregulates the

expression of genes involved in cooperative activities and increases production of AIs in a positive feed-forward mechanism (62, 63). QS systems have been identified in many bacterial species and Gram-positive and Gram-negative bacteria have been shown to use different QS systems (55).

In many Gram-negative bacteria, quorum sensing is primarily carried out by LuxI/LuxR-type systems that use AHLs as the AIs (Figure 1-4) (55). The LuxI homolog is an AHL synthase (64). The acyl chains of AHLs produced by different bacteria vary in length (C_4-C_{18}), degree of saturation, and oxidation at the third carbon position (Figure 1-5) (65). This diversity in AHL structures is the basis of specific intraspecies communication (54). AHLs diffuse freely through the inner and outer membranes, accumulating in the environment and cytoplasm as the population increases (54, 55). Above a threshold concentration, AHLs bind to the LuxR homolog receptor, which is a cytoplasmic transcription factor (66). AHL binding promotes LuxR homodimerization and binding to a DNA sequence called the *lux* box in the promoter region of target genes (67, 68). AHL-bound LuxR also induces expression of *luxI*, resulting in a feed-forward mechanism that further increases AHL concentration (63).

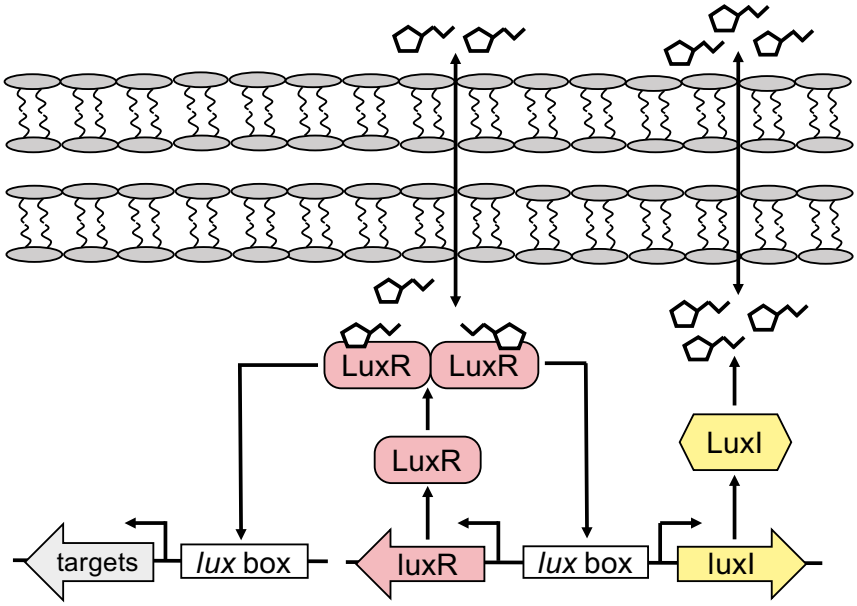

Figure 1-4. AHL-mediated quorum sensing in Gram-negative bacteria.
Gram-negative bacteria primarily use LuxI/LuxR-type quorum sensing systems, which employ *N*-acylhomoserine lactones (AHLs) as the autoinducer. The LuxI homolog (pink) is an AHL synthase and the LuxR homolog (yellow) is a cytoplasmic AHL receptor. AHLs diffuse freely through the inner and outer membranes of Gram-negative bacteria. Above a threshold concentration, AHLs bind to LuxR, resulting in dimerization and binding to specific DNA sequences called *lux* boxes in the promoters of target genes and the *luxI* gene.

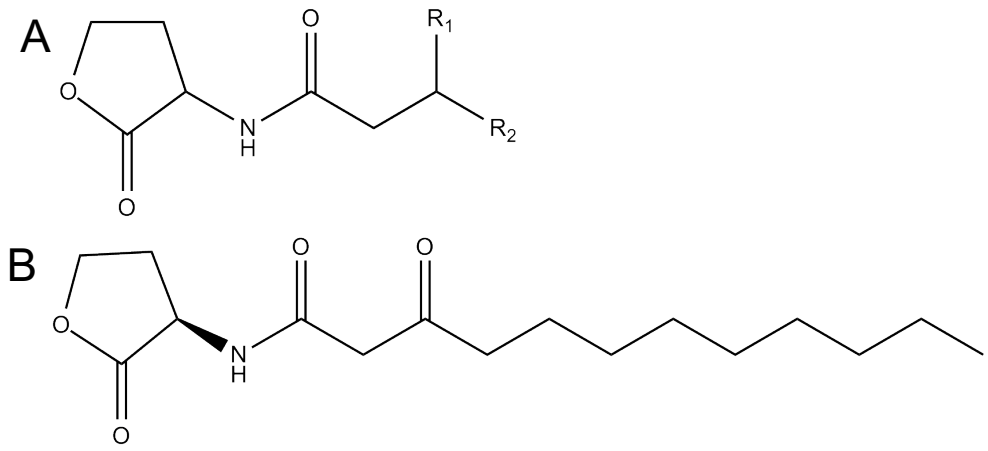

Figure 1-5. Structures of AHLs.
(A) General structure of an AHL and, as an example, (B) the structure of 3-oxo-C_{12}-HSL, an AHL produced by *P. aeruginosa*.

1.4.2 *N*-acylhomoserine lactone acylase family

The AHL acylases (EC 3.5.1.97) are another class of enzymes within the Ntn-hydrolase superfamily (Figure 1-2) (21, 69). These enzymes use serine as the N-terminal catalytic residue and assume a heterodimeric quaternary structure (70). AHL acylases catalyze hydrolysis of the amide bond in AHLs, releasing homoserine lactone and a fatty acid (69, 71). AHL acylases have been identified in both Gram-negative and Gram-positive bacteria, despite the fact that the latter do not contain AHL-based QS systems (21).

One function proposed for the AHL acylases involves disruption of quorum sensing, which is known as quorum quenching (21). AHLs are also susceptible to degradation by spontaneous reactions such as lactonolysis (72), thus enzymatic degradation of AHLs is not the only method of destroying these signaling molecules. Nevertheless, AHL acylases may contribute to normal turnover of AHLs in an endogenous QS system to ensure that signaling is arrested when the bacterial population density decreases or may be involved in fine-tuning the magnitude of the QS signal (21). AHL acylases produced by bacteria that do not express an AHL-dependent QS system may function in modulating the QS signaling of other species within a complex community to influence community behaviour (73). Alternatively, AHL acylases may aid Gram-positive bacteria in escaping the toxicity of AHLs (21). Finally, several groups have suggested based on the substrate flexibility of the AHL acylases that AHLs may not be the physiological substrates of these enzymes (21, 74).

1.4.3 Cross-reactivity between CG hydrolases and AHL acylases

Based on the structural and catalytic similarities between the AHL acylases and PVAs, the potential for cross-reactivity between these enzymes was proposed (75). An AHL acylase from *P. aeruginosa* that cleaves AHLs with C_6-C_{14} side chains and has low activity towards penicillin V

was later identified (44). Furthermore, Sunder *et al.* (2017) identified two homotetrameric PVAs from Gram-negative plant pathogenic bacteria that hydrolyze penicillin V as well as AHLs with C_6-C_{12} side chains. These enzymes are the first examples of PVAs or any other cysteine Ntn-hydrolases capable of degrading AHLs. When added to a culture of *P. aeruginosa,* the two PVAs were found to decrease the 3-oxo-C_{12}-HSL concentration and the levels of two virulence factors regulated by the QS system (45). These observations raise the possibility that AHL degradation may represent the physiological function of some PVAs.

1.5 Hydrolysis of siderophores

1.5.1 Siderophores used by *S. aureus*

Iron is a nutrient that pathogenic bacteria, including *S. aureus*, must acquire from the human host during infection (76). *S. aureus* possesses several mechanisms for iron acquisition, including heme uptake and the production and uptake of siderophores (76). Siderophores are high-affinity iron chelators that are capable of extracting Fe(III) from host extracellular iron-binding proteins (77). They are synthesized and secreted by a wide range of microorganisms and some bacteria can import siderophores produced by other species (termed xenosiderophores) in addition to their endogenous siderophores (76). Fe(III)-siderophore complexes are captured by specific cell surface receptors and are transported into the bacterial cell by cognate ABC transporters (78). *S. aureus* synthesizes two siderophores, called staphyloferrin A (SA) and staphyloferrin B (SB), and expresses uptake systems for various xenosiderophores, including enterobactin, bacillibactin, ferrichrome, desferrioxamine B, and aerobactin (Figure 1-6). Transcription of all *S. aureus* siderophore biosynthesis and uptake systems is upregulated under iron-limiting conditions by the ferric uptake regulator (Fur) (79).

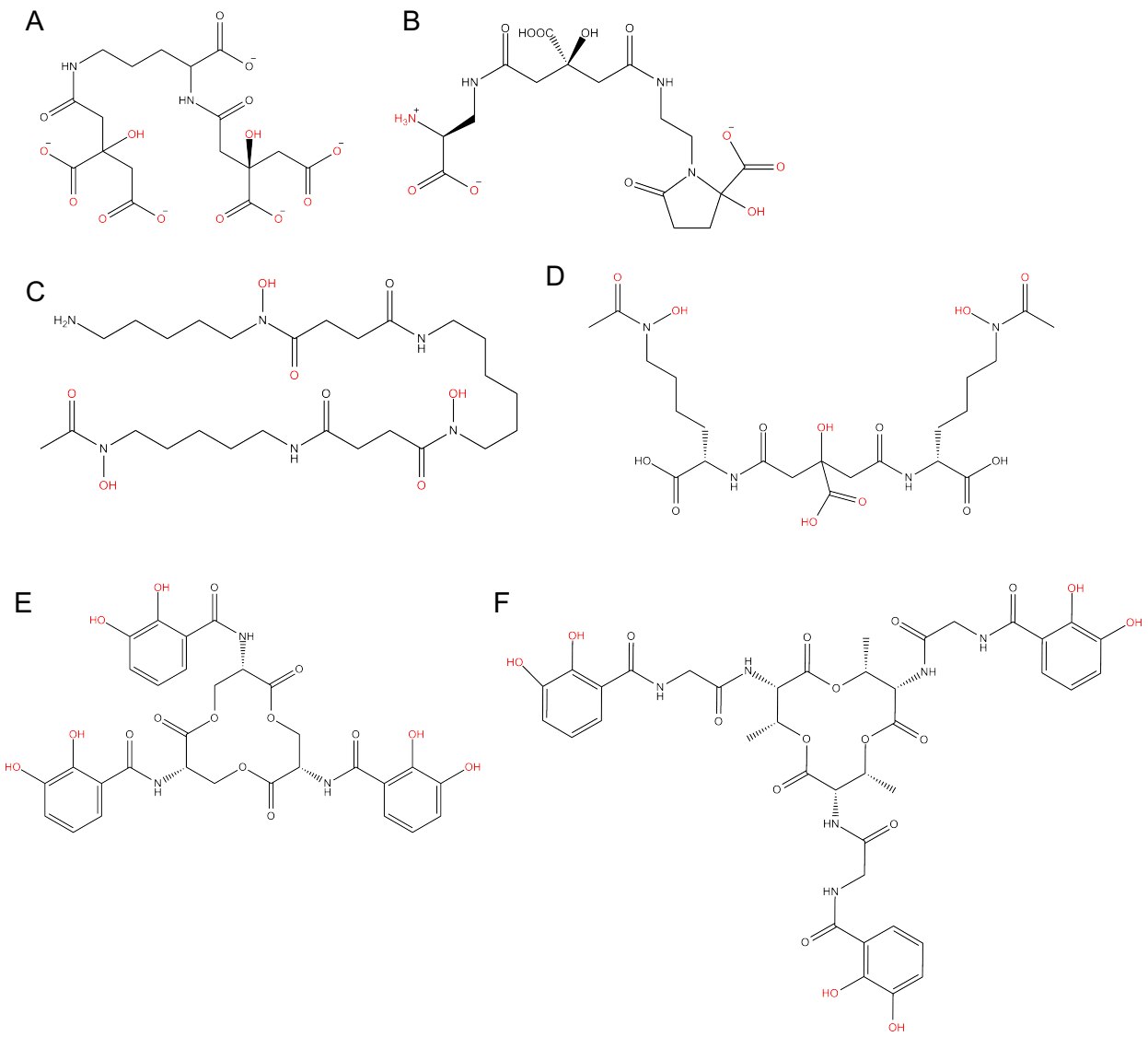

Figure 1-6. Structures of select siderophores used by *S. aureus*.
(A) Staphyloferrin A (SA) and (B) staphyloferrin B (SB) are endogenous siderophores. *S. aureus* also uses several xenosiderophores, including (C) desferrioxamine B, (D) aerobactin, (E) enterobactin and (F) bacillibactin. Functional groups that directly coordinate Fe^{3+} are coloured red.

1.5.2 Iron release from siderophores

Compared to the well-understood processes of siderophore biosynthesis and uptake, relatively little is known about the mechanisms of iron release from siderophores within *S. aureus*. Two major mechanisms for the liberation of iron from siderophores have been observed in other

organisms. The most common mechanism involves reduction of the chelated Fe(III) to ferrous iron [Fe(II)], which is then spontaneously released because siderophores have lower affinity for Fe(II) (77, 80). Following iron release, the siderophore scaffold may be modified (81). The other mechanism involves hydrolysis of the Fe(III)-bound siderophore by specialized enzymes, reducing the complex stability and facilitating Fe(III) release (80). Fe(III) may be subsequently reduced to Fe(II) or may interact with cellular iron-binding proteins (80). To date, only two *S. aureus* proteins involved in iron release from siderophores have been identified. The oxidoreductase IruO is encoded by a Fur-regulated gene and is required for *S. aureus* growth on Fe(III)-desferrixoamine B as a sole iron source (82). IruO binds Fe(III)-desferrioxamine B and Fe(III)-ferrichrome and facilitates NADPH-dependent Fe(II) release from these hydroxamate-type siderophores through a single-electron transfer mechanism (83). The Fur-regulated gene *ntrA* encodes a nitroreductase that is required for Fe(III)-SA utilization by *S. aureus* (82). No direct evidence for the function of NtrA is available because attempts to recombinantly express NtrA have failed. Further investigation into the mechanisms of iron liberation from siderophores in *S. aureus* is required.

1.5.3 SAUSA300_0269 expression correlates with siderophore-related genes

Mäder *et al.* (2016) used tiling arrays to perform a large-scale analysis of the *S. aureus* transcriptome under 44 different experimental conditions. Co-expressed genes were then identified using hierarchical cluster analysis (84). Genes encoding most characterized iron uptake systems were grouped into clusters B36 and B81, which fall within the larger C19 cluster (Figure 1-2). The gene of interest in this study, SAUSA300_0269, falls into cluster B81 and is correlated with genes encoding siderophore biosynthesis and uptake systems (Figure 1-7) (84). A search for transcription factor binding sites revealed that transcription of SAUSA300_0269 is likely Fur-regulated (84). These findings suggest that the protein of interest in this study may hydrolyze siderophores.

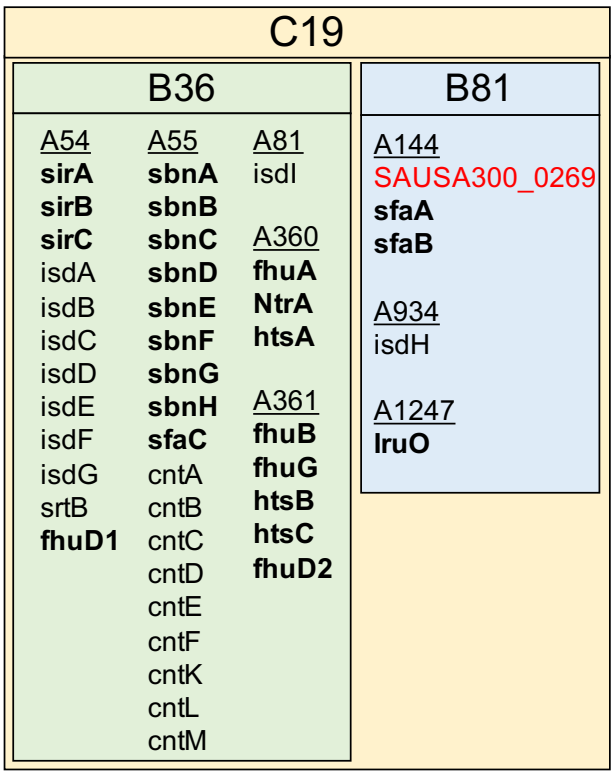

Figure 1-7. Expression of SAUSA300_0269 is correlated with the expression of siderophore-related genes.
Mäder *et al*. (2016) performed a large-scale analysis of the *S. aureus* transcriptome under many different growth conditions. The group employed hierarchical cluster analysis to identify co-expressed genes. Genes associated with most known iron-uptake systems fall into clusters B81 and B36, within the larger C19 cluster. Characterized genes in the B81 and B36 clusters are indicated. The gene SAUSA300_0269 (red font) falls into cluster B81 and its expression is correlated with that of genes involved in siderophore biosynthesis and uptake (bold).

1.6 Objectives

S. aureus is a major human pathogen that can cause severe disease and presents a risk to individuals in both healthcare and community settings. The increasing prevalence of multidrug-resistant strains underscores the need for novel therapeutics against *S. aureus*. The protein of interest in this study may be involved in important bacterial processes that are potential targets for drug development.

Based on phylogenetic analysis, the Ntn-hydrolase encoded by SAUSA300_0269 likely has penicillin V acylase activity. PVAs have significant value in the pharmaceutical industry, but the biological function of these enzymes is unknown. The objective of this study is to identify the physiological substrate(s) of the Ntn-hydrolase and determine its function in *S. aureus*. The Ntn-hydrolase will be henceforth referred to as *Sa*PVA, which is in keeping with the naming convention used for other characterized PVA enzymes.

Cross-reactivity between PVAs and AHL acylases has been observed and some AHLs inhibit growth and antagonize quorum sensing in *S. aureus*. I hypothesize that *Sa*PVA hydrolyzes AHLs and that this enzyme protects *S. aureus* from AHL-mediated toxicity. Expression of *Sa*PVA is correlated with expression of *S. aureus* genes involved in siderophore uptake and biosynthesis, suggesting that this enzyme may hydrolyze an amide bond in one or more siderophores. Therefore, I hypothesize that an alternative or additional function of *Sa*PVA is hydrolysis of siderophores to liberate iron for use by *S. aureus*. This study will provide insight into an industrially-important class of enzymes and potentially the mechanism by which *S. aureus* protects itself against AHL-mediated toxicity or liberates iron from Fe(III)-siderophores.

I tested the enzymatic activity of *Sa*PVA towards penicillin V, the bile salt glycocholic acid, two siderophores, and various AHLs. I determined that *Sa*PVA has PVA activity and hydrolyzes several AHLs. No activity was observed towards the other tested substrates. I examined the role of *Sa*PVA in protecting *S. aureus* against AHL-mediated toxicity, but the experimental results did not support this function. I also solved the structure of *Sa*PVA using X-ray crystallography and performed docking studies to investigate the binding of penicillin V and AHLs to the enzyme active site.

Chapter 2: Methods

2.1 Bacterial strains and growth conditions

Bacterial strains used in this work are listed in Table 2-1. *E. coli* cultures were grown in Luria-Bertani (LB) broth or on LB-agar. Growth medium was supplemented with ampicillin (100 μg/mL) and chloramphenicol (30 μg/mL) when appropriate. *S. aureus* strains were grown in tryptic soy broth (TSB), Roswell Park Memorial Institute (RPMI)-1640 medium supplemented with 2.0 g/L sodium bicarbonate, or on TSB-agar. Growth medium was supplemented with chloramphenicol (10 μg/mL) when appropriate

Table 2-1. Bacterial strains used in this study

Bacterial strain	Description	Source
E. coli DH5α	Strain used for general cloning. Inserts are highly stable due to *rec*A1 mutation. High DNA yields and quality due to *end*A mutation.	Life Technologies
E. coli BL21(DE3)	Strain used for protein overexpression. Contains a chromosomal copy of the phage T7 RNA polymerase gene inducible by IPTG. Deficient in lon and ompT proteases.	Novagen
S. aureus USA300 JE2	USA300 LAC, a community-associated MRSA strain isolated from the Los Angeles county jail, cured of all plasmids.	Received from David Heinrichs (UWO)
S. aureus RN4220	Cloning strain that is restriction-deficient due to a mutation in the *sau1 hsdR* gene. Receives plasmids from *E. coli* for transformation into *S. aureus*.	Received from David Heinrichs (UWO)
S. aureus JE2Δ*sapva*	Strain USA300 JE2 with an *sapva* (locus tag SAUSA300_0269) deletion.	This study

2.2 Cloning and site-directed mutagenesis of *sapva*

Plasmids and primers used in this work are listed in Table 2-2 and Table 2-3, respectively. The *Sa*PVA nucleotide sequence (locus tag SAUSA300_0269) was synthesized in a pET52b(+) vector (GenScript) and the construct was confirmed by sequencing (GeneWiz Inc). The C2A variant was generated by site-directed mutagenesis using a single-primer method (85). A 5'-phosphorylated mutagenesis primer (Integrated DNA Technologies) and Phusion polymerase (NEB) were used to perform whole-plasmid PCR amplification. Thermostable Ampligase (Epicentre) was included in the PCR solution to ligate the newly-synthesized plasmid after each round of replication. Methylated and hemi-methylated DNA were digested by incubating PCR products with DpnI overnight at 37°C. The full digestion solution (14.5 μL) was transformed into *E. coli* DH5α cells by heat shock. Plasmid purified from DH5α cells was used to confirm the mutation with sequencing (GeneWiz Inc) and was transformed into *E. coli* BL21(DE3) cells by electroporation for recombinant protein expression.

Table 2-2. Plasmids used in this study

Plasmid	Description	Source/Reference
pET52b(+)	*E. coli* cloning and protein expression vector. Contains a strong T7*lac* promoter, an optimized RBS, a multiple cloning site, and an ampicillin resistance gene.	Novagen
pET52b-*sapva*	pET52b(+) containing a construct for recombinant expression of *Sa*PVA.	This study.
pET52b-*sapva*-C2A	pET52b(+) containing a construct for recombinant expression of an *Sa*PVA C2A variant.	This study.
pKOR1	An *E. coli*/*S. aureus* shuttle vector used for markerless allelic replacements in *S. aureus*. Enables rapid cloning via lambda recombination and selection by *ccdB* expression. Antisense *sec*Y RNA is employed for counter-selection.	Bae and Schneewind (2005)

Table 2-3. Primers used in this study

Primer	Sequence (5'→3')[a]	Description
sapva-C2A-mutagenesis	5'phos CCATAGCAATGGCCACAGGATTCAC	For C2A mutation of *sapva* construct in pET52b(+)
sapva-upstream-for	*GGGGACAAGTTTGTACAAAAAAGCAG GCT*ATAAAAGGTACTTCATGTCGACG	For amplification of ~1 kb region upstream of chromosomal *sapva* gene to construct deletion.
sapva-upstream-rev	GGACCT**CCGCGG**TGTTCTCACTCCTCT GTACC	
sapva-downstream-for	GGACCT**CCGCGG**CGATTGATAATGGA ATTTGGTTGA	For amplification of ~1 kb region downstream of chromosomal *sapva* gene to construct deletion.
sapva-downstream-rev	*GGGGACCACTTTGTACAAGAAAGCTG GGT*TGAGTAAACTGGTGAATTTTCAG	

[a]Red sequences indicate altered codons and underlined sequences denote the specific nucleotides changed relative to the *S. aureus* JE2 wild-type strain. Bolded sequences indicate restriction enzyme sites. Italicized sequences indicate the Gateway attB1 and attB2 recombination sites (Invitrogen).

2.3 Construction of an *sapva* deletion mutant

A markerless deletion of the gene encoding *Sa*PVA was constructed using the pKOR1 system described by Bae and Schneewind (86). Chromosomal DNA was purified from *S. aureus* JE2 and two sets of primers were used to amplify ~1 kb sequences immediately upstream and downstream of the gene. The PCR products were digested with *Sac*II, ligated together, and recombined into the pKOR1 plasmid using BP Clonase II (Invitrogen Gateway cloning system). The plasmid was transformed into *E. coli* DH5α cells using heat shock and verified with DNA sequencing. The pKOR1 plasmid was transformed into the intermediate strain *S. aureus* RN4420 and subsequently into strain JE2 using electroporation. The chromosomal deletion was generated using the inducible counterselection method described by Bae and Schneewind (2006) with minor modifications. An overnight culture of *S. aureus* JE2 containing the pKOR1 plasmid was grown in TSB supplemented with 10 μg/mL chloramphenicol (TSB_{Cm10}) at 30°C. A 5-μL aliquot of this culture was transferred to fresh TSB_{Cm10} and incubated for 6 hours at 30°C, then 2 hours at 32°C, and then overnight at 42.3°C. The overnight culture was plated on pre-warmed TSA_{Cm10} plates at 42°C overnight. Colonies were used to inoculate 5-mL overnight cultures in TSB with no antibiotics, which were incubated at 30°C. Dilutions of the overnight culture were plated on TSA plates supplemented with 250 ng/mL anhydrotetracycline and incubated at 30°C overnight. Colonies sensitive to chloramphenicol were identified and the chromosomal deletion was confirmed by colony PCR.

2.4 Recombinant expression and purification of *Sa*PVA and the C2A variant

*Sa*PVA and the catalytically-inactive C2A variant were overexpressed in *E. coli* BL21(DE3) cells. LB medium supplemented with 100 μg/mL ampicillin was inoculated with ~3 mL of overnight culture and incubated at 37° with shaking for 2-3 hours until an OD_{600} of 0.6-0.8 was reached. For expression of *Sa*PVA, the LB medium was also supplemented with 30 μg/mL chloramphenicol because the BL21(DE3) expression strain contained an additional plasmid that encodes a chloramphenicol resistance gene. Protein expression was induced with 1 mM isopropyl β-D-thiogalactopyranoside (IPTG) and the cultures were incubated overnight at 25°C with shaking at 200 rpm. Cells were harvested by centrifugation at 4,680 × g for 10 minutes and resuspended in 10 mM HEPES (pH 7.0), 2 mM TCEP on ice. Cells were lysed at 4°C with an EmulsiFlex-C5 homogenizer (Avestin) and insoluble material was pelleted by centrifugation at 10,000-15,000 × g for approximately 1 hour.

*Sa*PVA and the C2A variant were purified as previously described (87) with some modifications. The soluble lysate was filtered with a 0.45 μm syringe filter (Millex-HP), adjusted to 50% saturation with ammonium sulfate solution, and equilibrated for 30 minutes at 4°C. The solution was centrifuged at 26,892 × g for 15 minutes. The pellet was washed twice by resuspending in approximately half the original volume of 10 mM HEPES (pH 7.0), 2 mM TCEP, adjusting to 50% saturation with ammonium sulfate, and then centrifuging at 26,892 × g for 15 minutes. The pellet was resuspended in 10 mM HEPES (pH 7.0), 2 mM TCEP, 0.5 M ammonium sulfate and incubated on ice for 10 minutes. The solution was centrifuged and applied to a 6-mL Toyopearl Phenyl-650M column (Tosh Bioscience). Protein was eluted with a linear decreasing ammonium sulfate gradient (0.5 M to 0 M) and dialyzed or exchanged by ultrafiltration into 10

mM HEPES (pH 8.0), 2 mM TCEP. The proteins were further purified by anion exchange chromatography. The proteins were applied to a Source 15Q column (GE Healthcare) and eluted with a linear gradient of 0 to 0.5 M NaCl. Fractions containing protein were concentrated, dialyzed or exchanged by ultracentrifugation into 10 mM HEPES (pH 8.0), 2 mM TCEP, 200 mM NaCl, and applied to a Superdex 200 10/300 size-exclusion column (GE Healthcare). Purified protein was dialyzed or exchanged by ultrafiltration into 20 mM Tris (pH 7.5), 100 mM NaCl, 2 mM TCEP, concentrated to approximately 10 mg/mL, flash frozen, and stored at -70°C. SDS-PAGE was used to assess protein purity. Protein concentrations were measured using predicted extinction coefficients at 280 nm calculated by the ExPASy ProtParam tool (https://www.expasy.org/) based on their primary amino acid sequences.

2.5 Mass spectrometry of *Sa*PVA and the C2A variant

Mass spectrometry (Proteomics Core Facility, University of British Columbia) was used to assess the purity of *Sa*PVA and the C2A variant and confirm the removal of the Met1 residue. *Sa*PVA was analyzed on a Waters Xevo G2 QTOF mass spectrometer with electrospray ionization in the positive mode. The C2A variant was analyzed on an Agilent 6550 QTOF mass spectrometer.

2.6 Crystallization and structure determination of *Sa*PVA

*Sa*PVA was crystallized using sitting-drop vapour diffusion at room temperature. The reservoir contained 0.2 M trisodium citrate, 20% (w/v) PEG3350 and crystals formed in a 2-µL drop containing a 1:1 mixture of 10 mg/mL *Sa*PVA and reservoir solution. The crystal that produced the X-ray dataset used for structure solution was not cryoprotected and was instead flash frozen in liquid nitrogen immediately upon removal from the drop. Diffraction data was collected

at the Canadian Light Source (CLS) on beamline 08ID-1. The data were processed and scaled using XDS (88). Crystals were of space group *C121* with two molecules in the asymmetric unit. The molecular replacement model was prepared using the Phenix suite (89) program Sculptor (90) from the structure of a PVA from *Bacillus subtilis* (PDB ID: 2OQC; 33% sequence identity). The molecular replacement phases were determined using Phaser-MR (91) and a preliminary model was generated using AutoBuild (632 of 658 residues built), both programs from the Phenix suite. Manual building was performed in Coot (92), and refinement was carried out with phenix.refine (89). The protein structure comparison service PDBeFOLD from the European Bioinformatics Institute (93) was used to compare the structure of *Sa*PVA with those of other PVAs. PyMOL (Version 1.7, Schrödinger, LLC) was used to produce structure figures.

2.7 Docking of penicillin V and AHLs to *Sa*PVA

Molecular docking was performed using the grid-based docking program AutoDock Vina (94). Three-dimensional structures of penicillin V and various AHLs were obtained from the PubChem compound database (https://pubchem.ncbi.nlm.nih.gov/). The ligand and *Sa*PVA receptor files were converted to PDBQT format using AutoDockTools (95). Waters were manually removed from the *Sa*PVA PDB file and chain B was used for docking. The ligand binding site was defined by a grid box centred at x = -20, y = 25, z = 18.5 with dimensions of 22 × 28 × 28 Å. Default values were used for all docking parameters.

2.8 Measurement of penicillin V acylase activity

PVA activity was measured by determining the amount of 6-APA released upon incubation of *Sa*PVA with penicillin V using an endpoint assay (96). Increasing concentrations (5 – 60 mM)

of the potassium salt of phenoxymethylpenicillinic acid (Sigma-Aldrich) were incubated with 0.5 μM *Sa*PVA in 0.1 M sodium phosphate (pH 6.0) in a total volume of 250 μL. After a four-minute incubation at 37°C, the reaction was arrested by adding 0.75 mL of 2.0 M sodium acetate (pH 2.5). The solution was centrifuged at maximum speed for 1 minute to remove precipitated protein. Production of 6-APA was detected by adding 0.25 mL of 0.25% *p*-diaminobenzaldehyde (*p*DAB; Sigma-Aldrich) in methanol. *p*DAB reacts with 6-APA to form a coloured Schiff's base. Colour was allowed to develop for 2 minutes at room temperature and then the absorbance of the solution at 415 nm was measured on a Varian CARY 50 UV-Vis spectrophotometer. A standard curve was used to quantify the 6-APA produced. All assay measurements were performed in triplicate. A Michaelis-Menton model was fit to the data using non-linear regression in GraphPad Prism 7.

2.9 Bile salt hydrolase activity assay

The bile salt hydrolase activity of *Sa*PVA was assayed colourimetrically by measuring the amount of glycine released upon incubation of the enzyme with 50 mM sodium glycocholate hydrate (Sigma) in 0.1 M sodium phosphate (pH 6.0). After incubating at 37°C for approximately 4 hours, the 100-μL reaction solution was centrifuged in a Nanosep 3K centrifugal filter device (Pall Corporation) at 14,000 × g to remove the enzyme. The filtrate was mixed with an equal volume of a 2% (w/v) ninhydrin solution and boiled for 15 minutes. The absorbance at 570 nm was measured. A standard curve indicated that glycine concentrations of ≥ 600 μM are reliably detected by the assay.

2.10 Measurement of AHL acylase activity

The AHL acylase activity of *Sa*PVA was measured by determining the amount of L-homoserine lactone (HSL) produced upon incubation of the enzyme with various AHLs using a fluorescamine colourimetric assay. Fluorescamine reacts with the primary amine group of HSL to produce a fluorescent product. Reaction solutions contained 0.1 M sodium phosphate (pH 6.0), 2 mM of each AHL and 5 μM *Sa*PVA in a total volume of 40 μL. The AHLs tested include: C_4-HSL, C_6-HSL, 3-oxo-C_6-HSL, C_8-HSL, 3-oxo-C_8-HSL, C_{10}-HSL, and 3-oxo-C_{12}-HSL (Cayman Chemicals). After a 30-minute incubation at 37°C, 140 μL of 0.2 M sodium acetate (pH 4.5) was added. The solution was centrifuged at 14,000 × g in a Nanosep 3K centrifugal filter device (Pall Corporation) to remove the enzyme. To the filtrate, 20 μL of 1 mg/mL fluorescamine in acetone was added and the solution was incubated for 1 hour at room temperature. Absorbance at 380 nm was recorded. All assay measurements were performed in triplicate.

2.11 *S. aureus* growth in the presence of 3-oxo-C_{12}-HSL

Bacterial growth in the presence of 3-oxo-C_{12}-HSL was measured in both TSB and RPMI-1640 medium. For both experiments, single colonies of wild-type *S. aureus* JE2 and the *sapva* deletion strain were inoculated into TSB and the cultures were incubated overnight at 37°C. To test growth in RPMI medium, overnight cultures were pelleted and the bacteria were washed with RPMI medium. The cultures were then diluted 1/20 into fresh RPMI medium and incubated for 3 hours at 37°C. The morning subcultures were further diluted to an OD_{600} of 0.005 in 1 mL of RPMI medium in a 24-well plate. In appropriate wells, 3-oxo-C_{12}-HSL was added to a final concentration of 75 μM or 100 μM. Cultures were grown in a TECAN plate reader for ~24 hours at 37°C. Every

3 minutes, the plate was subjected to a 10-second linear shake followed by a 10-second orbital shake and the OD_{600} was measured. To test growth in TSB, the same protocol was used with two alterations: 1) the pellet wash step was removed because all subsequent cultures were also prepared with TSB, and 2) 3-oxo-C_{12}-HSL was added to the 1-mL cultures to a final concentration of 100 μM or 250 μM. For both experiments, the bacterial growth curves were plotted as the average growth for three technical replicates and error bands represent the standard deviation.

2.12 Fe(III)-enterobactin iron release assay

*Sa*PVA hydrolysis of Fe(III)-enterobactin was assayed by monitoring iron release from Fe(III)-enterobactin after incubation with the enzyme. Fe(III)-enterobactin was prepared by incubating enterobactin dissolved in DMSO with $FeCl_3$ in 1 mM HCl at room temperature for 2 hours. Enterobactin and $FeCl_3$ were mixed in a 1.2:1 ratio to avoid introducing excess iron into the solution. A reaction solution containing 0.1 M HEPES (pH 6.8), 80 μM Fe(III)-enterobactin, and 10 μM *Sa*PVA was prepared and absorbance at 495 nm was measured on a Varian CARY 50 UV-Vis spectrophotometer before and after incubation for 3 hours at 37°C. A ferrozine assay (97) was used to detect any Fe^{3+} released from Fe(III)-enterobactin. Following the incubation with *Sa*PVA, 1 mM ascorbate and 1 mM ferrozine were added to the reaction solutions to reduce Fe^{3+} and detect the resulting Fe^{2+}. Reaction solutions were centrifuged at maximum speed for 1 minute to remove precipitated protein and incubated for an additional 1 hour at room temperature for colour development. Reaction of Fe^{2+} with ferrozine was detected by measuring the absorbance at 562 nm. A standard curve indicated that Fe^{3+} concentrations as low as 5 μM are reliably detected by this assay.

2.13 HPLC assay of enterobactin hydrolysis

The activity of *Sa*PVA towards enterobactin and Fe(III)-enterobactin was assayed by HPLC. One reaction solution contained 0.1 M HEPES (pH 6.8), 300 μM enterobactin, 10 μM *Sa*PVA and the other contained 0.1 M sodium phosphate (pH 6.0), 300 μM Fe(III)-enterobactin, and 10 μM *Sa*PVA. Both reaction solutions were incubated with and without the enzyme at 37°C for 3 hours. A 10-μL aliquot of each sample was injected onto a Waters XTerra C18 reversed-phase 5 μm column (2.1 mm × 150 mm) on an Infinity 1260 Quaternary HPLC system (Agilent). Enterobactin was eluted with a linear gradient of 10-50% acetonitrile in water over 30 minutes at a flow rate of 0.5 mL/min. Both solvents were supplemented with 0.1% TFA. Enterobactin was detected by its absorbance at 220 nm.

2.14 HPLC assay of Fe(III)-SA hydrolysis

SA was produced by incubating the biosynthetic enzymes SfaD and SfaB with precursors required for its synthesis as previously described (98). The reaction solution contained 50 mM HEPES (pH 7.3), 2 mM citrate, 1 mM D-ornithine, 5 mM ATP, 0.5 mM $MgCl_2$, 5 μM SfaD, and 5 μM SfaB. Following overnight incubation at room temperature, the reaction solution was centrifuged in a Nanosep 10K centrifugal filter device (Pall Corporation) at 14,000 × g for 14 minutes to remove the enzymes. To the filtrate, $FeCl_3$ prepared in 1 mM HCl was added to a final concentration of 3 mM. The solution was then centrifuged at 18,000 × g to remove precipitates and filtered with a 0.2 μm Iso-Disc filter (Supelco).

The SA solution was then incubated with and without 10 μM *Sa*PVA at 37°C for 5.5 hours. The enzyme was added directly to an aliquot of the SA solution to ensure that SA is present in the

highest possible concentration, which is approximately 1 mM if the biosynthetic reaction went to completion. HEPES buffer is present in the SA solution, thus no additional buffer was added.

After the incubation, a 50-μL aliquot was removed from each reaction solution and mixed with an equal volume of acetonitrile. Each 100-μL sample was injected onto a Waters XBridge 3.5 μm Amide column (2.1 mm × 100 mm) on an Infinity 1260 Quaternary HPLC system (Agilent). Fe(III)-SA was eluted with a linear decreasing gradient of 95-50% acetonitrile in 1.25 mM ammonium acetate (pH 5.1) over 20 minutes. Fe(III)-SA was detected by its absorbance at 340 nm.

Chapter 3: Results

3.1 *Sa*PVA is a penicillin V acylase

Based on phylogenetic and binding-site analysis of the CG hydrolase family, *Sa*PVA was identified as a probable PVA (32, 33). This enzyme was expected to hydrolyze penicillin V and display low or no activity towards bile salts. Steady-state kinetic parameters for the PVA activity of *Sa*PVA were determined by measuring the initial velocity of 6-APA production using a *p*DAB assay (Figure 3-1). A control reaction was carried out with the *Sa*PVA C2A mutant, confirming that this variant is catalytically inactive. The K_m, k_{cat}, and k_{cat}/K_m values for *Sa*PVA are: 16.5 ± 1.9 mM, 6.9 ± 0.3 min^{-1}, and 0.42 ± 0.07 mM^{-1} min^{-1}, respectively. The K_m value for *Sa*PVA is comparable with those of other characterized PVAs, which range from approximately 2–45 mM (Table 3-1). The k_{cat} and k_{cat}/K_m values for characterized PVAs vary over two orders of magnitude and the *Sa*PVA values fall at the low end of the range for both k_{cat} and k_{cat}/K_m (Table 3-1).

The BSH activity of *Sa*PVA was tested to determine if this enzyme shows any cross-reactivity with bile salts. Hydrolysis of glycocholic acid was measured using ninhydrin to detect the glycine produced by this reaction. The ninhydrin assay is capable of detecting a turnover of as little as 1% of the glycocholic acid in the reaction solution. After a 3-hour incubation with *Sa*PVA, however, no glycine production was detected, which suggests that *Sa*PVA has no activity towards this substrate.

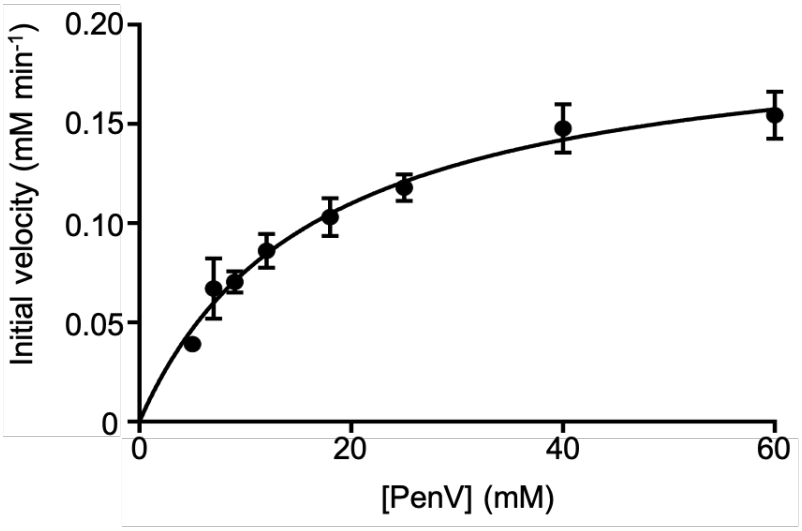

Figure 3-1. Steady-state kinetics of penicillin V hydrolysis by *Sa*PVA.
The rate of penicillin V (PenV) hydrolysis was measured by quantifying the 6-APA product using a *p*DAB assay. *Sa*PVA (0.5 μM) was incubated with various concentrations of penicillin V in 0.1 M sodium phosphate (pH 6.0) at 37°C. A Michaelis-Menton model was fit to the data using non-linear regression. Error bars represent the standard deviation of three independent experiments.

Table 3-1. Steady-state kinetic parameters of PVAs from various organisms

Organism	K_m (mM)	k_{cat} (min^{-1})	k_{cat}/K_m (mM^{-1} min^{-1})	Temp. (°C)	pH	Reference
Staphylococcus aureus	16.5 ± 1.9	6.9 ± 0.3	0.42 ± 0.07	37	6.0	This work
Bacillus sphaericus	11	45.5[a]	4.1	37	5.8	Olsson *et al.* (1985)
Bacillus subtilis	–	11.7[a]	–	40	6.6	Rathinaswamy *et al*. (2005),
Streptomyces mobaraensis	5.2 ± 0.7	270.8 ± 11	51.9	37	7.0	Zhang *et al.* (2007)
Streptomyces lavendulae	2.05	60.25	38.88	40	8.0	Torres *et al*. (2002)
Fusarium sp. SKF235	10	76.8	7.7	55	6.5	Sudharkaran and Shewale (1995)
Pectobacterium atrosepticum	40.8 ± 8.5	–	–	45	5.0	Avinash *et al.* (2015)
Agrobacterium tumefaciens	45.8 ± 17.0	–	–	45	6-7	Avinash *et al.* (2017)

–, not available.
[a]k_{cat} values were calculated from reported specific activity values by Zhang *et al.* (2007).

3.2 *Sa*PVA hydrolyzes some AHLs

*Sa*PVA is a member of the CG hydrolase family which, along with the AHL acylases, are part of the larger Ntn-hydrolase superfamily. Based on a previous report of two PVAs from Gram-negative bacteria that possess AHL acylase activity (45) and the structural similarities between penicillin V and AHLs, a range of AHLs were tested as substrates of *Sa*PVA. AHL hydrolysis was measured using a fluorescamine assay to detect the primary amine in the L-homoserine lactone (HSL) product. All AHLs were incubated with *Sa*PVA for 30 minutes and the HSL produced was

quantified using a standard curve. *Sa*PVA hydrolyzed C_6-HSL and all tested AHLs with a chain length of eight or more carbons and demonstrated a preference for AHLs with no 3-oxo-substitution (Table 3-2).

Measurement of the specific activity of AHL hydrolysis by *Sa*PVA under the conditions tested was not possible due to the limited solubility of longer-chain AHLs. AHLs with acyl chains of eight carbons or more are only sparingly soluble in aqueous solvents. Thus, while each AHL was added to the reaction mixture at a theoretical concentration of 2 mM, the proportion that is soluble and available to interact with *Sa*PVA is unknown and likely decreases as the acyl chain length increases. As a result, it is not possible to determine from this data if C_8-HSL is the AHL hydrolyzed most readily by *Sa*PVA, or if the enzyme has a preference for longer-chain AHLs, but their solubility is limiting.

Table 3-2. Concentration of L-HSL produced by hydrolysis of various AHLs by *Sa*PVA

AHL substrate	Concentration of L-HSL detected (μM)[a]
C_4-HSL	0
C_6-HSL	87 ± 12
3-oxo-C_6-HSL	0
C_8-HSL	1500 ± 150
3-oxo-C_8-HSL	470 ± 70
C_{10}-HSL	640 ± 180
3-oxo-C_{12}-HSL	230 ± 70

[a]After incubation with *Sa*PVA for 30 min.

3.3 *Sa*PVA does not protect *S. aureus* against 3-oxo-C_{12}-HSL-mediated toxicity

Long-chain AHLs (C_{10}-C_{14}) with a 3-oxo substitution inhibit *S. aureus* growth and antagonize its quorum sensing system (99). To investigate the potential function of *Sa*PVA in protecting *S. aureus* against AHL-mediated toxicity, growth of the wild-type JE2 strain and a Δ*sapva* strain were monitored in the presence of 3-oxo-C_{12}-HSL. This AHL is produced by *P. aeruginosa*, a bacterium that may inhabit the same environment as *S. aureus*. In a study of two PVAs from Gram-negative bacteria with AHL acylase activity, both hydrolyzed 3-oxo-C_{12}-HSL and the enzymes inhibited *P. aeruginosa* quorum sensing phenotypes (45). Growth inhibition by 3-oxo-C_{12}-HSL is expected to be exacerbated in the Δ*sapva* strain if *Sa*PVA functions to detoxify AHLs.

S. aureus growth experiments were first conducted with liquid cultures in RPMI medium because the highest levels of *sapva* transcription are observed when *S. aureus* is grown in this medium (84). *S. aureus* was grown in the presence and absence of 3-oxo-C_{12}-HSL, which was added to the cultures at concentrations previously shown to completely inhibit *S. aureus* growth. In RPMI medium, however, growth of the JE2 and Δ*sapva* strains was not affected by the presence of 3-oxo-C_{12}-HSL (Figure 3-2A).

In an attempt to reproduce the *S. aureus* growth inhibition phenotype, liquid cultures in rich TSB medium were used to conduct the same experiment. In TSB, growth of both *S. aureus* strains was inhibited by 3-oxo-C_{12}-HSL in a concentration-dependent manner (Figure 3-2B). Within the error of the experiment, the same level of growth inhibition was experienced by the JE2 and Δ*sapva* strains, which does not support a role for *Sa*PVA in protecting *S. aureus* from the toxic effects of 3-oxo-C_{12}-HSL.

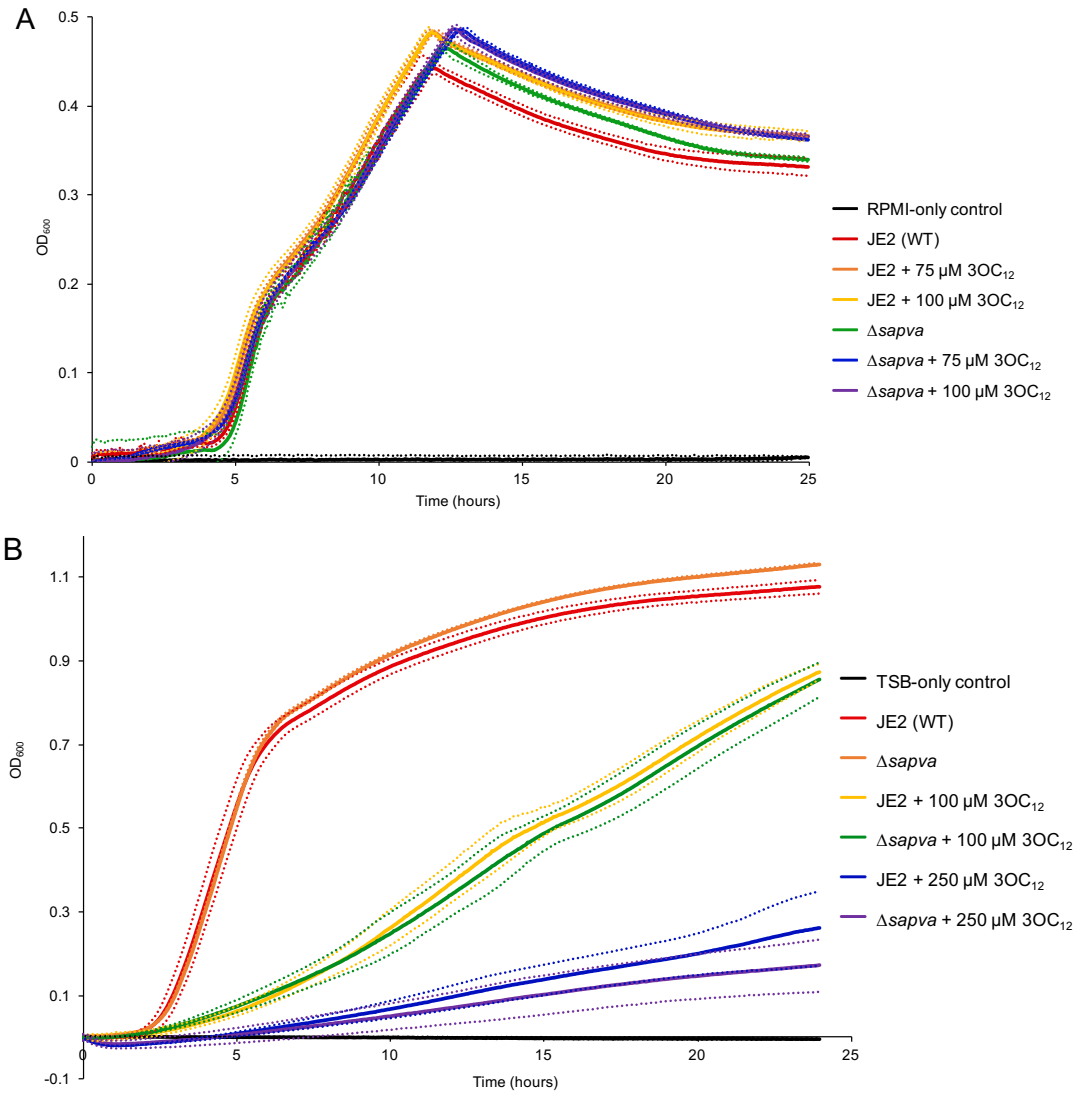

Figure 3-2. Effect of 3-oxo-C_{12}-HSL on growth of *S. aureus* JE2 and Δ*sapva*.
Liquid cultures of *S. aureus* JE2 (wild-type) and Δ*sapva* were inoculated at an OD_{600} of 0.005 into the appropriate medium. Cultures were incubated at 37°C for ~24 hours and the OD_{600} was read every three minutes following a 20 second shake. (A) Cultures were grown in RPMI medium and some were supplemented with 75 µM or 100 µM 3-oxo-C_{12}-HSL ($3OC_{12}$). The RPMI-only control curve is shown in black. Growth curves for strain JE2 in the presence of 0, 75, and 100 µM 3-oxo-C_{12}-HSL are shown in red, orange, and yellow, respectively. Growth curves for strain Δ*sapva* in the presence of 0, 75, and 100 µM 3-oxo-C_{12}-HSL are shown in green, blue, and purple, respectively. (B) Cultures were grown in TSB and some were supplemented with 100 µM or 250 µM 3-oxo-C_{12}-HSL. The TSB-only control curve is shown in black. Growth curves for strain JE2 in the presence of 0, 100, and 250 µM 3-oxo-C_{12}-HSL are shown in red, yellow, and blue, respectively. Growth curves for strain Δ*sapva* in the presence of 0, 100, and 250 µM 3-oxo-C_{12}-HSL are shown in orange, green, and purple, respectively. Growth curves are the average of three replicates and dashed lines represent the upper and lower limits of one standard deviation.

3.4 *Sa*PVA does not hydrolyze enterobactin or Fe(III)-enterobactin

Enterobactin is a siderophore imported by *S. aureus* that is noted for its extremely high affinity for iron (100). In *E. coli*, iron release from enterobactin requires cleavage of the siderophore by the esterase Fes (101). No Fes homolog is present in *S. aureus* and I hypothesized that, instead, *Sa*PVA hydrolyzes the amide bonds linking the catechol groups to the serine-trilactone scaffold to facilitate iron release from enterobactin.

Hydrolysis of Fe(III)-enterobactin by *Sa*PVA was first tested by measuring iron release. Solutions of Fe(III)-enterobactin appear red and absorb light at 495 nm. The A_{495} of Fe(III)-enterobactin was measured before and after incubation with *Sa*PVA and no decrease in absorbance was observed. A ferrozine assay was then used to detect iron released from Fe(III)-enterobactin. Ascorbate was added to reduce iron to the Fe^{2+} form, which subsequently reacts with ferrozine to produce a complex that absorbs at 562 nm. The ferrozine assay is sensitive enough to detect iron concentrations corresponding to iron release from as little as 6% of the Fe(III)-enterobactin, but no free iron was detected following a 3-hour incubation with *Sa*PVA.

Enterobactin was analyzed by HPLC using a reversed-phase C_{18} column and detected by its absorbance at 220 nm (102). Enterobactin and Fe(III)-enterobactin were incubated with and without *Sa*PVA and analyzed by HPLC to determine if *Sa*PVA hydrolyzes the siderophore, as indicated by a change in retention time. At the low pH used for HPLC analysis (pH ~2), enterobactin cannot bind Fe^{3+}, thus apo enterobactin is the species eluted from the column in both cases. For both enterobactin and Fe(III)-enterobactin, HPLC traces of the samples incubated with and without the enzyme contain no significant differences (Figure 3-3), suggesting that this siderophore is not hydrolyzed by *Sa*PVA. A peak corresponding to DMSO elutes at ~6.1 min and enterobactin elutes at ~22.3 min in each trace. Regardless of the presence of *Sa*PVA, extended

incubation at 37°C produces a small peak at ~18.3 min in the traces of both enterobactin and Fe(III)-enterobactin and also a shoulder on the enterobactin peak for the former. These peaks likely correspond to degradation products.

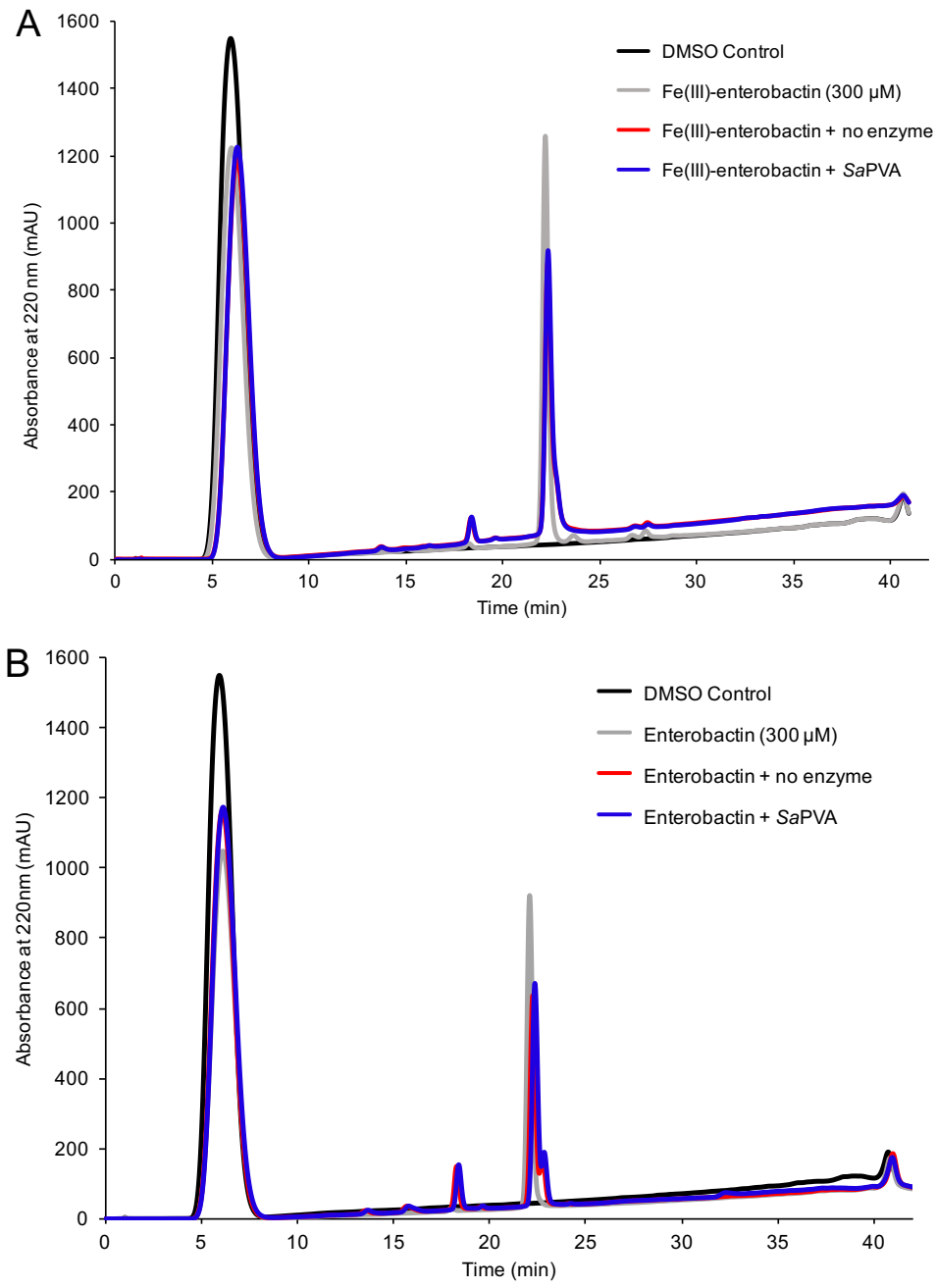

Figure 3-3. HPLC assay of Fe(III)-enterobactin and enterobactin hydrolysis by SaPVA. (A) Fe(III)-enterobactin and (B) Enterobactin (300 µM) were incubated with and without 10 µM *Sa*PVA at 37°C for 3 hours. An aliquot of each reaction solution was injected onto a reversed-phase C_{18} column. Enterobactin was eluted from the column with an increasing acetonitrile gradient. The HPLC trace of a DMSO control is shown in black. Traces shown in gray correspond to 300 µM Fe(III)-enterobactin or enterobactin not subjected to incubation at 37°C. Traces shown in blue and red correspond to Fe(III)-enterobactin or enterobactin incubated with and without *Sa*PVA, respectively.

3.5 *Sa*PVA does not hydrolyze staphlyoferrin A

SA is another siderophore for which the mechanism of iron release is unknown and it contains three amide bonds that could be hydrolyzed by *Sa*PVA to facilitate iron release. SA was produced *in vitro* by incubating the biosynthetic enzymes, SfaB and SfaD, with the required precursors and cofactors. A control reaction was prepared, from which the second enzyme in the biosynthetic pathway, SfaB, was excluded. Following removal of the biosynthetic enzymes and addition of iron to SA, the reaction mixture was incubated with or without *Sa*PVA. A sample of each solution was analyzed by HPLC using an amide column and Fe(III)-SA was detected at 340 nm (98).

Analysis of the reaction mixture from which SfaB was excluded confirms that the peak that elutes at ~17.6 minutes corresponds to Fe(III)-SA. The smaller peak that elutes at 17.8 min in the trace of the reaction mixture lacking SfaB corresponds to absorbance from ATP that was not consumed by SfaD. No change in retention time of the Fe(III)-SA peak is observed between samples incubated with and without *Sa*PVA for 5.5 hours (Figure 3-4), suggesting that *Sa*PVA does not hydrolyze Fe(III)-SA.

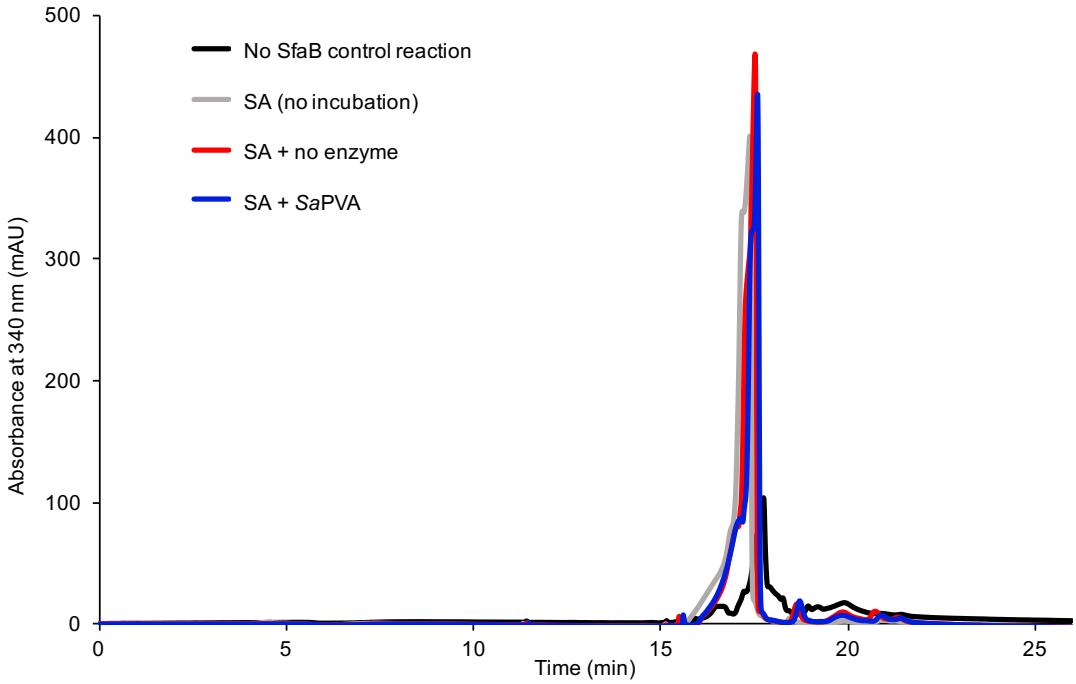

Figure 3-4. HPLC assay of Fe(III)-SA hydrolysis by *Sa*PVA.
SA was produced by incubating the biosynthetic enzymes, SfaB and SfaD, with the required substrates. $FeCl_3$ was added to produce Fe(III)-SA and the reaction solution was incubated with or without 10 μM *Sa*PVA at 37°C for 5.5 hours. An aliquot was mixed with acetonitrile and injected onto an amide column. Fe(III)-SA was eluted with a decreasing acetonitrile gradient. The HPLC trace shown in black corresponds to a control SA reaction solution from which SfaB was excluded and the gray trace corresponds to the Fe(III)-SA reaction solution. HPLC traces shown in blue and red correspond to the SA reaction solution incubated with and without *Sa*PVA.

3.6 Structure of *Sa*PVA

To gain insight into the substrates that may be accommodated by the *Sa*PVA binding pocket, the structure of *Sa*PVA was solved. The structure of a PVA from *Bacillus subtilis* (*Bsu*PVA; 2OQC), which shares 33% sequence identity with *Sa*PVA, was used for phasing by molecular replacement. *Sa*PVA crystallized in space group *C121* with two protomers (Figure 3-5A) in the asymmetric unit. The structure was determined to a resolution of 1.9 Å. Data collection and refinement statistics are summarized in Table 3-3. For chains A and B, 329 and 327 residues of the total 330 were modelled, respectively, with 98% of residues in the most favoured regions of

the Ramachandran plot. The N-terminal catalytic cysteine (Cys2) was modelled and no density corresponding to Met1 was observed. Positive electron density in the difference map (F_o-F_c) surrounding the Cys2 sulfur atom suggests that partial oxidation of this atom may have occurred. Oxidation at Cys2 was previously observed in the crystal structure of the PVA from *Bacillus sphaericus* (PDB ID: 2PVA) (47).

The structure of the *Sa*PVA protomer is consistent with the overall fold conserved among Ntn-hydrolases. The core contains two antiparallel β-sheets, which are packed together and sandwiched between two layers of α-helices. Members of the Ntn-hydrolase superfamily vary in their topology beyond the conserved αββα core, but all characterized PVAs share the same arrangement of secondary structure elements. *Sa*PVA is composed of a five-stranded β-sheet packed against an eight-stranded β-sheet, with a pair of α-helices on either side. The catalytic cysteine residue forms the start of one core β-strand. *Sa*PVA shares high structural similarity with other characterized PVAs (Table 3-4). For example, superposition of *Sa*PVA with *Bsu*PVA (2OQC) using PDBeFOLD, gives a root mean square deviation (RMSD) of 1.38 Å over 312 aligned Cα atoms.

The two *Sa*PVA protomers in the asymmetric unit are related by two-fold rotational symmetry and form a dimer. The stable tetrameric structure characteristic of PVAs is formed by association with another dimer, which is related to the first by a crystallographic twofold axis (Figure 3-5B). The *Sa*PVA structure also contains the "assembly motif" typical of PVAs from Gram-positive bacteria. The assembly motif is a loop comprising residues 186-222 that stabilizes the tetrameric structure by extending out approximately 28 Å from each protomer and interacting with the protomer positioned across from it diagonally.

Mass spectrometry data (not shown) and the absence of electron density corresponding to Met1 in the *Sa*PVA crystal structure indicate that this residue was removed. The mass spectrum of the *Sa*PVA C2A variant confirms that Met1 was also removed in the absence of the catalytic cysteine. Most Ntn-hydrolases require processing to remove a leader sequence and expose the N-terminal catalytic residue. *Sa*PVA does not require autocatalytic processing to produce the mature enzyme, which is consistent with findings for other PVAs from Gram-positive bacteria (47, 49, 50). Instead, the *N*-formyl methionine was likely removed by a methionyl aminopeptidase during recombinant expression.

Superposition of residues identified as essential for catalysis in *Bsu*PVA (Cys2, Arg17, Asp20, Tyr82, Asn175, Arg228) (32) with the homologous residues in *Sa*PVA revealed that the active site architecture is highly conserved (Figure 3-6). *Sa*PVA is therefore expected to share a common catalytic mechanism with characterized PVAs.

Four loops important for substrate binding in previously characterized PVAs (33) are also present in *Sa*PVA. These loops comprise residues 22-29 (loop 1), 59-63 (loop 2), 127-140 (loop 3), and 257-273 (loop 4). Superposition of the four substrate-binding loops of *Sa*PVA with those of two other PVAs from Gram-positive bacteria, *Bsu*PVA (2OQC) and *Bsp*PVA (3PVA), reveals that the orientation of these loops is similar in all three structures (Figure 3-7A). More significant differences are observed when the substrate-binding loops of *Sa*PVA are overlaid with those of PVAs from Gram-negative bacteria (Figure 3-7B). In particular, loop 4 is oriented more inside the binding pocket closer to the catalytic cysteine, and loop 3 is positioned further from loop 2 in PVAs from Gram-negative bacteria. These observations suggest that PVAs from Gram-positive bacteria could bind similar substrates, while PVAs from Gram-negative bacteria may bind different substrates.

Table 3-3. Data collection and refinement statistics for *Sa*PVA

Data Collection	
Resolution range (Å)	47.75 – 1.90 (2.00 – 1.90)[a]
Space group	*C121*
Unit cell dimensions	
a, b, c (Å)	114.74, 75.9, 97.94
α, β, γ (°)	90, 123.68, 90
Unique reflections	55,024 (8,398)
Completeness (%)	99.4 (98.3)
Redundancy	6.4 (4.73)
Average $I/\sigma I$	13.69 (2.62)
R_{meas}	7.00 (56.30)
CC1/2	99.8 (87.2)
Wilson B factor (Å^2)	37.25
Refinement	
R_{work} (R_{free})	0.1880 (0.2344)
Number of water molecules	
r.m.s.d bond length (Å)	0.010
Average *B*-values (Å^2)	45.42
Ramachandran plot (%)	
Most favoured regions	97.85
Disallowed regions	0.0

[a]Values in parentheses are for data in the highest resolution shell.

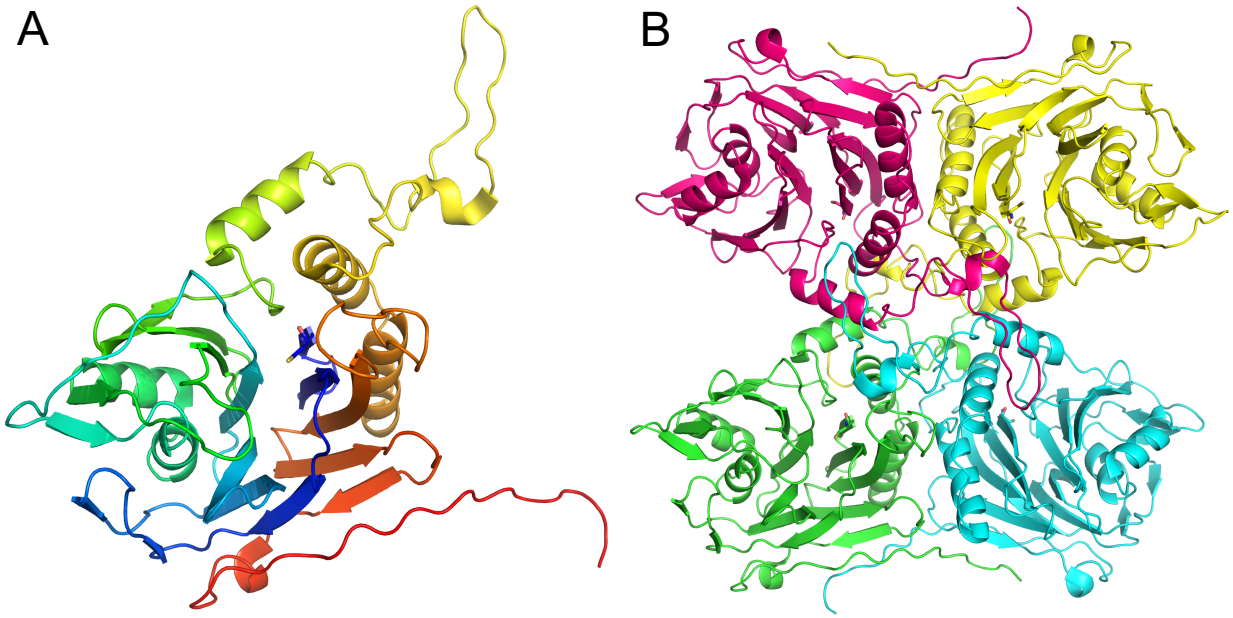

Figure 3-5. Crystal structure of the *Sa*PVA protomer and tetramer.
(A) *Sa*PVA protomer shown in cartoon representation and coloured with a gradient from blue (N-terminus) to red (C-terminus). (B) Cartoon representation of the tetrameric assembly of *Sa*PVA. Promoters are shown in pink, yellow, green, and cyan. In both structures, the nucleophilic N-terminal cysteine residues (Cys2) are shown in stick representation.

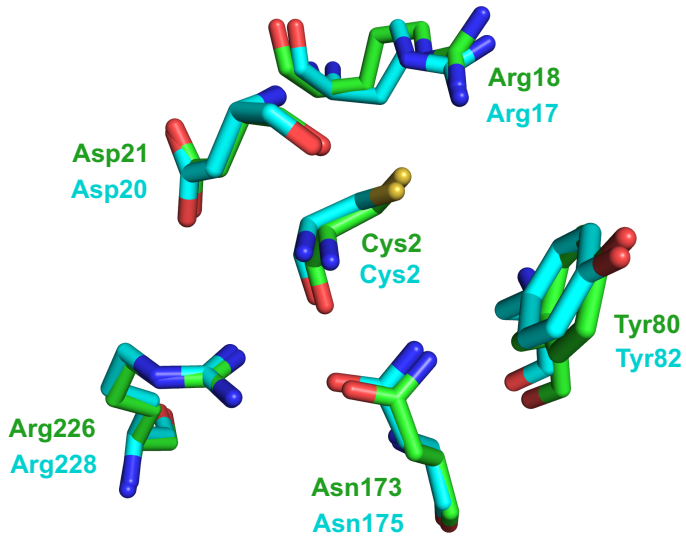

Figure 3-6. Superposition of active site residues from *Sa*PVA and *Bsu*PVA.
Active site residues of *Sa*PVA and *Bsu*PVA (PDB ID: 2OQC) are shown in stick representation with their carbon atoms coloured green and cyan, respectively. Oxygen, nitrogen, and sulfur atoms are coloured blue, red, and yellow, respectively.

Table 3-4. Structural similarity of *Sa*PVA to other PVAs

PVA	Bacterium	RMSD (Å)	Fraction of residues aligned	Sequence identity over aligned residues (%)	PDB ID
*Bsu*PVA	*Bacillus subtilis*	1.38	312/317	33	2OQC
*Bsp*PVA	*Bacillus sphaericus*	1.73	315/328	28	3PVA
*Pa*PVA	*Pectobacterium atrosepticum*	1.90	275/326	20	4WL2
*At*PVA	*Agrobacterium tumefaciens*	1.92	262/317	19	5J9R

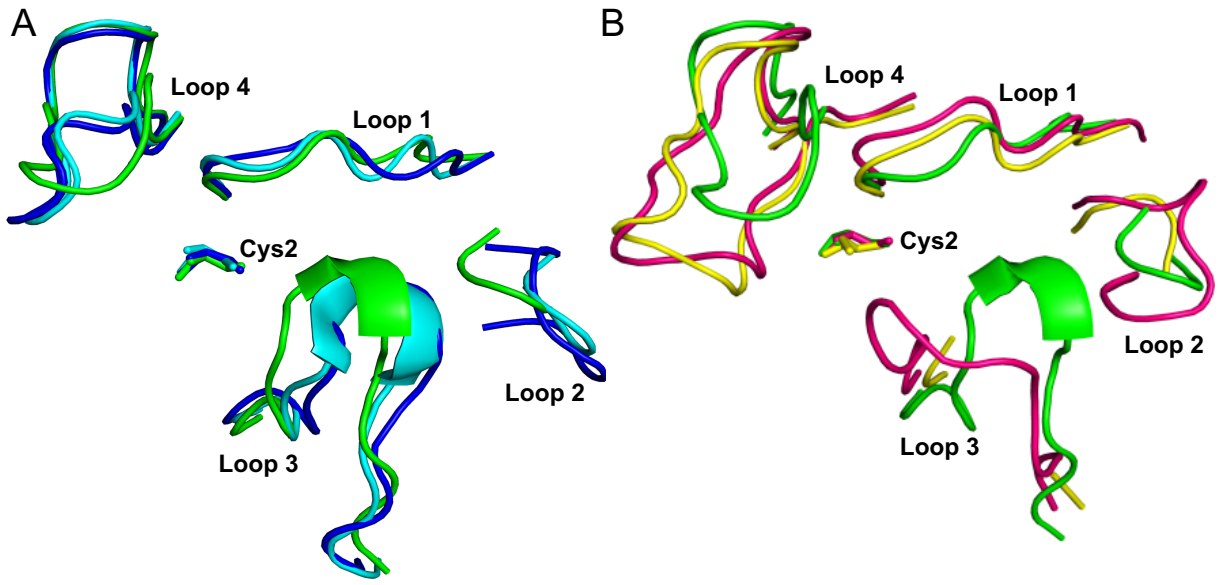

Figure 3-7. Superposition of binding pocket loops from *Sa*PVA and other PVAs.
(A) *Sa*PVA binding loops (green) overlaid with those of two PVAs from Gram-positive bacteria: *Bsu*PVA (cyan; 2OQC) and *Bsp*PVA (blue; 3PVA). (B) *Sa*PVA binding loops (green) overlaid with those of two PVAs from Gram-negative bacteria: *Pa*PVA (pink; 4WL2) and *At*PVA (yellow; 5J9R). Loop3 is not modelled in the structure of *At*PVA. Loops are shown in cartoon representation and the nucleophilic Cys2 residues are shown in stick representation.

3.7 Docking of penicillin V and AHLs to the *Sa*PVA structure

The binding modes of penicillin V and AHLs to *Sa*PVA were studied to identify the structural features important for interaction with binding pocket residues, which may inform predictions of other potential substrates. Attempts to co-crystallize the *Sa*PVA C2A variant with penicillin V were unsuccessful and co-crystallization with AHLs was not attempted due to the limited aqueous solubility of these substrates. Instead, the binding modes of penicillin V and AHLs were investigated by docking these substrates to the *Sa*PVA active site *in silico* using AutoDock Vina.

In the top penicillin V binding mode (calculated affinity of -6.7 kcal/mol), the phenyl ring forms π-π stacking interactions with the conserved Tyr80 residue and the β-lactam and thiazolidine rings are positioned closer to the entrance of the binding pocket (Figure 3-8A). Of the top nine binding modes calculated by AutoDock Vina, six involve this π-π stacking interaction, suggesting that it may be important for penicillin V binding. In the top binding mode, the carbonyl carbon of the scissile amide bond is positioned 5.9 Å from the sulfur atom of Cys2. Both the catalytic residue and substrate would need to undergo conformational changes to allow for nucleophilic attack. Penicillin V is positioned such that the carbonyl carbon can form a hydrogen bond with the side chain of Arg226. This observation is consistent with previous results for the docking of penicillin V to another PVA (53) and suggests that Arg226 contributes to the oxyanion hole. The position of penicillin V does not allow for formation of a hydrogen bond between the carbonyl carbon and the side chain of Asn173. This residue was expected to contribute to the oxyanion hole based on studies of the homologous residue in BSHs (33, 52). Therefore, the top molecular docking solution represents a reasonable penicillin V binding mode, but some key interactions are absent.

For molecular docking of AHLs to *Sa*PVA, the predicted binding modes were not consistent between 3-oxo-substituted and unsubstituted AHLs. In the top binding mode for each unsubstituted AHL, the HSL ring is positioned deep within the binding pocket and the acyl chain points out towards the Cys2 residue (Figure 3-8B). For C_8-HSL (-6.3 kcal/mol), the carbonyl carbon is located 8.9 Å from the sulfur atom of Cys2. In contrast, in the top binding mode for each 3-oxo-AHL, the HSL ring is positioned near the entrance of the binding site in the same pocket that was occupied by the β-lactam and thiazolidine rings of penicillin V (Figure 3-8C). The acyl chain extends into the binding pocket. This binding mode is consistent with previous docking results for both substituted and unsubstituted AHLs (21, 45, 103). Unique to this dockings study, however, is the observation that the 3-oxo groups is oriented towards the backbone N–H group of Cys2. For 3-oxo-C_{12}-HSL (-5.7 kcal/mol), the carbonyl carbon is positioned 7.3 Å from the Cys2 sulfur atom.

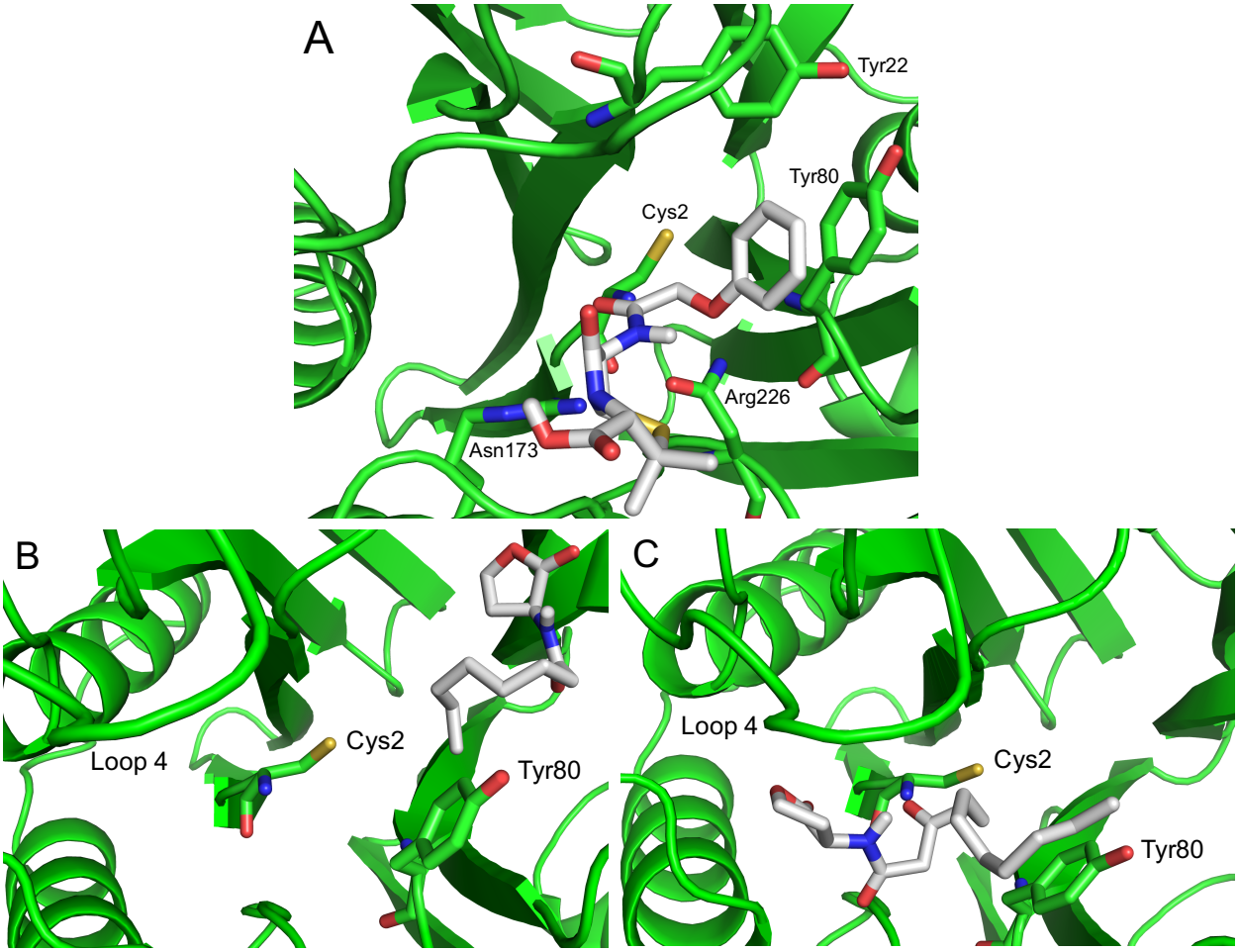

Figure 3-8. Molecular docking of penicillin V and AHLs to the active site of *Sa*PVA. Top solution for molecular docking of (A) penicillin V, (B) C_8-HSL, and (C) 3-oxo-C_{12}-HSL to the *Sa*PVA active site. *Sa*PVA is shown in cartoon representation and coloured green. Key active site residues are shown in stick representation. The carbon backbone of penicillin V is coloured gray. Oxygen, nitrogen, and sulfur atoms are coloured red, blue, and yellow, respectively.

Chapter 4: Discussion

4.1 Identification of *Sa*PVA substrates

To date, several PVAs have been biochemically characterized and the structures of four of these enzymes, two from Gram-positive bacteria and two from Gram-negative bacteria, have been solved (45, 47, 104, 105). A range of substrates similar to penicillin V have been tested with these PVAs, including penicillin G, ampicillin, cephalosporins, and capsaicin (106, 107). In most cases, however, the relevance of these substrates to the physiological function of the PVA was not considered.

*Sa*PVA was annotated as a CG hydrolase and was identified by two groups as a probable penicillin V acylase based on bioinformatics analyses of the CG hydrolase family (32, 33). *In vitro* activity assays showed that *Sa*PVA hydrolyzes penicillin V, while no BSH activity towards glycocholic acid was observed. This lack of BSH activity by *Sa*PVA is consistent with the observation that *Bsu*PVA also lacks BSH activity (105). Of the characterized PVAs, *Bsu*PVA shares the highest sequence similarity with *Sa*PVA and Kumar *et al*. (2006) determined that the PVA and BSH activities within the family are reflected in the primary amino acid sequence (25). The presence of BSH activity towards taurine-linked bile salts, however, cannot be ruled out as another *Sa*PVA homolog, *Bsp*PVA, has some activity towards taurocholic acid, but not glycocholic acid (25).

To gain insight into the physiological functions of *Sa*PVA, the activity of the enzyme towards several substrates was tested. Based on a study of two PVAs from Gram-negative bacteria that possess AHL acylase activity (45), various AHLs were tested and found to be hydrolyzed by *Sa*PVA. This enzyme is the first reported PVA from a Gram-positive bacterium that also possesses AHL acylase activity. This finding is discussed in detail in Section 4.2.

This study is also the first in which siderophores are considered as potential substrates of a PVA. The enzyme PvdQ produced by *P. aeruginosa*, however, is an AHL acylase that also hydrolyzes an amide bond in a precursor to the siderophore pyoverdine (103). A recent *S. aureus* transcriptome study identified *Sa*PVA as a Fur-regulated gene for which expression is enhanced under the same conditions that increase transcription of siderophore-related genes (84). This finding prompted tests of *Sa*PVA activity towards the siderophores enterobactin and SA, but neither was hydrolyzed under the conditions tested.

Enterobactin was hypothesized as the most likely siderophore substrate of *Sa*PVA due to previous observations that cleavage of this siderophore is required for iron release (101) and the absence of an enterobactin esterase homolog in the *S. aureus* genome. Furthermore, enterobactin and penicillin V share some structural similarities. Although enterobactin is significantly larger than penicillin V, both molecules contain an aromatic moiety on the carbonyl side of the amide bond and the nitrogen atom of the amide bond is directly attached to a ring structure. In contrast, SA contains no aromatic groups or ring structures and the nitroreductase NtrA was shown to play a role in Fe(III)-SA utilization, although the mechanism is unknown (82). Transcription of the *Sa*PVA gene, however, clustered most closely with that of genes involved in SA biosynthesis and secretion (84). *S. aureus* imports several other siderophores containing at least one amide bond that have not yet been tested as substrates of *Sa*PVA, including SB, desferrioxamine B, ferrichrome, aerobactin, and bacillibactin.

4.2 AHL acylase activity of *Sa*PVA

4.2.1 Determination of AHL acylase activity *in vitro*

An *in vitro* activity assay confirmed the hypothesis that *Sa*PVA hydrolyzes some AHLs. *Sa*PVA shows a preference for unsubstituted AHLs with an acyl chain of six or more carbons, which is consistent with the preferences observed by the two Gram-negative PVAs that possess AHL acylase activity (45). Among other enzymes classified as AHL acylases, however, some share these preferences, while others are active against short-chain AHLs (21).

A limitation of the assay used to detect AHL acylase activity was the inability to accurately report the kinetic parameters due to the poor aqueous solubility of longer-chain AHLs. Obtaining an estimate of the specificity constant (k_{cat}/K_m) of *Sa*PVA for AHLs would be beneficial for two reasons. Firstly, the specificity constants would indicate which AHL is the preferred substrate of *Sa*PVA. Since different bacteria use different AHLs as their primary quorum sensing molecules, this information would inform hypotheses about the function of the enzyme. Secondly, the specificity constants for AHL hydrolysis could be compared with those of *Sa*PVA for other types of substrates. A significantly higher specificity constant for AHL hydrolysis than penicillin V hydrolysis, for example, would support the hypothesis that AHLs are the physiological substrate of *Sa*PVA.

4.2.2 Function of *Sa*PVA AHL acylase activity *in vivo*

*Sa*PVA was hypothesized to protect *S. aureus* from AHL toxicity based on previous reports of long-chain AHLs inhibiting the growth of *S. aureus* and antagonizing its QS system (99). Growth experiments in TSB medium did not support a role for *Sa*PVA in protecting the bacterium from the toxic effects of 3-oxo-C_{12}-HSL. Protection against two other long-chain AHLs that inhibit *S. aureus* growth, 3-oxo-C_{10}-HSL and 3-oxo-C_{14}, could also be tested with this assay. The

observation that unsubstituted AHLs are preferred by *Sa*PVA while 3-oxo-substitued AHLs are more efficient in *S. aureus* growth inhibition (99), suggests that protection from AHL-mediated toxicity may not be the physiological function of the enzyme. An alternate hypothesis is that *Sa*PVA hydrolyzes AHLs to provide *S. aureus* a competitive advantage by disrupting quorum sensing by Gram-negative bacteria in its environment. For example, *S. aureus* and *P. aeruginosa* are found together in the cystic fibrosis lung environment (108). Unsubstituted AHLs are the primary QS molecules used by some Gram-negative bacteria, including *Burkholderia cenocepacia*, another important pathogen in cystic fibrosis (109).

Interestingly, the AHL growth inhibition phenotype was not observed when the experiment was carried out in RPMI medium. AHL-mediated growth inhibition has been proposed to involve perturbation of the bacterial membrane potential, however the exact mechanism of action is unknown (99). Evidence also supports the existence of a specific, saturable membrane receptor to which 3-oxo-C_{12}-HSL binds (99). Saroj *et al.* (2017) investigated the inhibition of *Streptomyces pyogenes* growth by 3-oxo-C_{12}-HSL and 3-oxo-C_{14}-HSL and determined that both glucose and iron (25 μM) were strictly required for the growth inhibition phenotype to be observed (110). Both TSB and RPMI medium contain glucose, but RPMI medium contains only trace amounts of iron. Iron may be required for AHL-mediated disruption of the membrane potential or for expression or function of the membrane receptor. Alternatively, iron-dependent growth inhibition may be a result of the conversion of some of the 3-oxo-C_{12}-HSL to its tetramic acid derivative, which occurs via an irreversible, non-enzymatic and base-catalyzed reaction (111, 112). The tetramic acid derivative also has antibacterial activity against Gram-positive bacteria and has been shown to bind iron (111). For different tetramic acids, iron binding has been shown to enhance or attenuate their antibacterial activity (113). In TSB media, the tetramic acid derivative may sequester

sufficient iron to reduce the growth rate of *S. aureus*. For *S. aureus* growing in RPMI medium, which already contains only trace iron, no growth inhibition would be observed. Alternatively, the tetramic acid may actually be the molecule mediating growth inhibition, and it may be more active when complexed with iron.

The localization of *Sa*PVA in *S. aureus* is unclear. *Sa*PVA does not possess a signal peptide and therefore it has been suggested to be cytoplasmic (47, 114), while characterized PVAs from Gram-negative bacteria contain a signal peptide (33). Reports of AHL transport into the *S. aureus* cytoplasm could not be found in the literature, but 3-oxo-C_{12}-HSL is transported into *S. pyogenes*, another Gram-positive bacterium, potentially by a siderophore uptake protein (110). Therefore, *Sa*PVA may interact with AHLs in the cytoplasm.

4.3 Structural characterization of *Sa*PVA and substrate docking

The overall structure of *Sa*PVA was consistent with the known fold of Ntn-hydrolases and the active site configuration is nearly identical to that in other PVAs. An assembly motif was present in the *Sa*PVA structure as expected, but the reason that this tetramer-stabilizing loop is present only in PVAs from Gram-positive bacteria is not understood.

Superposition of the entire structure of *Sa*PVA with other PVAs indicated high structural similarity, thus the substrate-binding loops were selected for closer investigation to determine if *Sa*PVA may bind a unique ligand. On the contrary, the loops were similar in size and orientation for all three PVAs from Gram-positive bacteria, suggesting that these PVAs bind similar types of substrates. Therefore, the physiological substrate(s) of these enzymes are likely molecules that may be encountered by all of the environmental or pathogenic Gram-positive bacteria that encode a PVA. A unique siderophore only imported by one species is thus less likely to be the

physiological substrate. This observation does not, however, mean that all of the Gram-positive PVAs bind the exact same substrate. Koch *et al*. (2014) determined that the substrate specificity of an AHL acylase could be altered by mutating just two residues (103). Due to the relatively low sequence similarity between Gram-positive PVAs (~30%), they may bind similar but distinct molecules.

One co-crystal structure of penicillin V bound to a PVA has been deposited in the PDB. A *Bsp*PVA C1G variant was crystallized with two molecules in the asymmetric unit and penicillin V bound in both active sites (PDB ID: 2Z71). In one active site, the orientation of penicillin V is similar to that observed in the top binding mode for *Sa*PVA. Notably, the penicillin V phenyl group forms π-π stacking interactions with the *Bsp*PVA Tyr82 residue. In the other active site, however, no π-π stacking interactions are observed. This structure has not been described in the literature, nor have the structure factors been submitted to the PDB. Therefore, it is difficult to perform a critical analysis of this co-crystal structure. In a previous report of penicillin V docking to *Bsu*PVA, the penicillin V phenyl group formed π-π stacking interactions with the *Bsu*PVA Tyr82 residue (33). Based on the presence of these π-π stacking interactions in docking results for both *Sa*PVA and *Bsu*PVA, I propose that an aryl ring may be a structural feature present in the physiological substrate of *Sa*PVA.

Docking of various AHLs to *Sa*PVA produced an unexpected result: two distinct binding modes were observed for unsubstituted and 3-oxo-substituted AHLs. Several groups have docked AHLs to Ntn hydrolases, including to two Gram-negative PVAs (21, 45, 103). In previous docking studies, all AHLs bound with the HSL ring positioned near the entrance of the binding pocket and the acyl chain extended deeper into the pocket. Therefore, this orientation more likely represents the true binding mode for AHLs. Docking of 3-oxo-AHLs to *Sa*PVA produced a similar docking

mode, except for the orientation of the 3-oxo group towards the backbone N–H group of Cys2. In the docked structures, the 3-oxo group impedes nucleophilic attack of the carbonyl carbon of the scissile amide bond. Therefore, while the overall orientation of the 3-oxo-AHLs is consistent with previous studies, the top binding mode is not catalytically feasible. Although a consistent AHL binding mode was not obtained, the molecular docking results suggest that an acyl chain can be accommodated in the *Sa*PVA binding pocket. Therefore, a fatty acid chain is another structural feature that may be present in the physiological substrate of *Sa*PVA.

A common structural feature of penicillin V and AHLs is the rings (two in penicillin V, one in AHLs) that bind near the entrance of the *Sa*PVA binding pocket. All substrates shown to be hydrolyzed by PVAs to date, including penicillin G, ampicillin, taurocholic acid, and capsaicin, contain one or more rings (25, 45, 115). Therefore, I propose that this structural feature may determine binding to the PVA active site. One or more rings are likely present in the physiological substrate of *Sa*PVA, with an aryl group or fatty acid chain on the other side of the amide bond.

4.4 Physiological function of *Sa*PVA

Despite the importance of PVAs in the pharmaceutical industry, their physiological function remains unknown. Several groups have proposed that the function of PVAs may be to degrade environmental phenolic compounds as a carbon source (36, 40). The most common phenolic compounds produced by the breakdown of plant matter, such as flavonoids and phenolic acids, however, do not contain an amide bond that could be hydrolyzed by PVAs (116, 117). Furthermore, transcription of *Sa*PVA has been shown to be upregulated in RPMI (84), a medium which contains glucose as a carbon source. This observation is inconsistent with expression of *Sa*PVA being unnecessary when glucose is plentiful. Therefore, it is more likely that the

physiological substrates of *Sa*PVA and the other PVAs are some type of secondary metabolite, such as an antibiotic or quorum sensing molecule, produced by the PVA-encoding species or by other microorganisms in their environment. PVAs may detoxify these molecules or their activity may in some way provide a selective advantage for the PVA-producer.

The most promising candidates for the physiological substrates of *Sa*PVA to emerge from this study are AHLs. *Sa*PVA may be involved in disrupting QS systems of Gram-negative bacteria with which they share an environment. Hydrolysis of siderophores in the bacterial cell to facilitate iron release has not been ruled out as the function of *Sa*PVA, however, enterobactin and SA are likely not the substrates of this enzyme. Of the other siderophores used by *S. aureus*, many do not contain aryl groups, only SB contains a small ring structure, and all have several polar substituents. Based on the observation that *Sa*PVA shows a preference for AHLs with an unsubstituted acyl chain, it is unlikely that any of these siderophores are hydrolyzed by the enzyme.

4.5 Conclusions

PVAs are industrially important enzymes that are also produced by a number of important bacterial pathogens, yet their physiological function remains unknown. In this study, the *S. aureus* enzyme *Sa*PVA was biochemically and structurally characterized. *Sa*PVA was confirmed to possess PVA activity, with no activity towards the bile salt glycocholic acid. This study is the first to show cross-reactivity between a PVA from a Gram-positive bacterium and AHLs. Growth experiments suggested that *Sa*PVA does not function in AHL detoxification, but the enzyme may function in degrading AHLs to disrupt Gram-negative QS systems and provide *S. aureus* a competitive advantage in mixed-species communities. Two siderophores, enterobactin and SA, are unlikely to be substrates of *Sa*PVA. Finally, the structure of the enzyme was solved and docking

studies with penicillin V and various AHLs were performed. The substrate-binding site of *Sa*PVA was compared with those of other PVAs and it was determined that the PVAs from Gram-positive bacteria likely bind similar substrates. Finally, several structural features which may be present in the physiological substrate were identified.

4.6 Future Directions

Further investigation of *Sa*PVA is required to identify physiological substrates and provide insight into the function of this enzyme. Firstly, the limitations in the AHL acylase assay will be addressed to obtained estimates of kinetic parameters for the activity of *Sa*PVA towards AHLs. Sunder *et al*. (2017) used a sensitive fluorescence-based assay to obtain a reasonable estimate of kinetic parameters by working at low AHLs concentrations (10-250 μM) to ensure solubility. With information about which AHLs are preferred by *Sa*PVA, the role of this AHL acylase activity will be tested *in vivo*.

To test the hypothesis that the physiological function of *Sa*PVA is interruption of the QS system of Gram-negative bacteria, the enzyme will be added to cultures of bacteria that use an AHL hydrolyzed by *Sa*PVA as their primary quorum sensing molecule. Firstly, a reduction in the concentration of that quorum sensing molecule in the medium will be measured using established methods (45). Furthermore, a decrease in the production of quorum-sensing regulated products, such as proteases or toxins, or a reduction in biofilm formation will be measured. Finally, a co-culture experiment will be carried out in which the bacterium of interest is cultured with either wild-type *S. aureus* or the Δ*sapva* strain and biofilm formation or production of QS-related products by the bacterium of interest is measured. The *sapva* deletion strain produced in this study

will be useful for testing many different phenotypes that may provide insight into the function of *Sa*PVA.

To determine whether other siderophores are likely to be substrates of *Sa*PVA, further analysis of the binding pocket will be carried out with bioinformatics tools to clarify whether polar groups are likely accommodated in the binding pocket. Fur-regulation of *Sa*PVA transcription will also be confirmed before proceeding with further siderophore studies.

Any promising findings obtained in studies of *Sa*PVA will be extended to other PVAs to shed light on the functions of this important enzyme family.

Bibliography

1. Tong SYC, Davis JS, Eichenberger E, Holland TL, Fowler VG (2015) Staphylococcus aureus Infections: Epidemiology, Pathophysiology, Clinical Manifestations, and Management. *Clin Microbiol Rev* 28(3):603–661.

2. Williams REO (1963) Healthy carriage of Staphylococcus aureus: its prevalence and importance. *Bacteriol Rev* 27(1):56–71.

3. Noble WC, Valkenburg HA, Wolters CHL (1967) Carriage of Staphylococcus aureus in random samples of a normal population. *J Hyg (Lond)* 65(4):567–573.

4. Casewell MW, Hill RLR (1986) Elimination of nasal carriage of Staphylococcus aureus with mupirocin ('pseudomonic acid')—a controlled trial. *J Antimicrob Chemother* 17(3):365–372.

5. Gordon RJ, Lowy FD (2008) Pathogenesis of methicillin-resistant Staphylococcus aureus infection. *Clin Infect Dis* 46(Suppl 5):S350–S359.

6. Wertheim HF, et al. (2005) The role of nasal carriage in Staphylococcus aureus infections. *Lancet Infect Dis* 5:751–762.

7. Lowy FD (1998) Staphylococcus aureus Infections. *N Engl J Med* 339(8):520–532.

8. Barber M, Rozwadowska-Dowzenko M (1944) Infection by penicillin-resistant staphylococci. *The Lancet* 2(6530):641–644.

9. Kirby WMM (1944) Extraction of a Highly Potent Penicillin Inactivator from Penicillin Resistant Staphylococci. *Science* 99(2579):452–453.

10. Livermore DM (2000) Antibiotic resistance in staphylococci. *Int J Antimicrob Agents* 16(Suppl 1):3–10.

11. Jevons MP (1961) "Celbenin"-resistant Staphylococci. *Br Med J* 1(5219):124–125.

12. Kluytmans-VandenBergh MFQ, Kluytmans JAJW (2006) Community-acquired methicillin-resistant Staphylococcus aureus: Current perspectives. *Clin Microbiol Infect* 12(Suppl. 1):9–15.

13. Goetghebeur M, Landry PA, Han D, Vicente C (2007) Methicillin-resistant Staphylococcus aureus: A public health issue with economic consequences. *Can J Infect Dis Med Microbiol* 18(1):27–34.

14. Chang S, et al. (2003) Infection with Vancomycin-Resistant Staphylococcus aureus Containing the vanA Resistance Gene. *N Engl J Med* 348(14):1342–1347.

15. Gardete S, Tomasz A (2014) Mechanisms of vancomycin resistance in Staphylococcus aureus. *J Clin Invest* 124(7):2836–2840.

16. Artymiuk PJ (1995) A sting in the (N-terminal) tail? *Nat Struct Biol* 2(12):1035–1037.

17. Brannigan JA, et al. (1995) A protein catalytic framework with an N-terminal nucleophile is capable of self-activation. *Nature* 378(6555):416–419.

18. Oinonen C, Rouvinen J (2000) Structural comparison of Ntn-hydrolases. *Protein Sci* 9:2329–2337.

19. Duggleby HJ, et al. (1955) Penicillin acylase has a single-amino-acid catalytic centre. *Nature* 373(6511):264–268.

20. Kim Y, Yoon K-H, Khang Y, Turley S, Hol WGJ (2000) The 2.0 A Crystal Structure of Cephalosporin Acylase. *Structure* 8(10):1059–1068.

21. Utari PD, Vogel J, Quax WJ (2017) Deciphering Physiological Functions of AHL Quorum Quenching Acylases. *Front Microbiol* 8:1123.

22. Smith JL (1995) Structures of glutamine amidotransferases from the purine biosynthetic pathway. *Biochem Soc Trans* 23(4):894–898.

23. Oinonen C, Tikkanen R, Rouvinen J, Peltonen L (1995) Three-dimensional structure of human lysosomal aspartylglucosaminidase. *Nat Struct Biol* 2(12):1102–1108.

24. Löwe J, et al. (1995) Crystal structure of the 20S proteasome from the archaeon T. acidophilum at 3.4 A resolution. *Science* 268(5210):533–539.

25. Kumar RS, et al. (2006) Structural and functional analysis of a conjugated bile salt hydrolase from Bifidobacterium longum reveals an evolutionary relationship with penicillin V acylase. *J Biol Chem* 281(43):32516–32525.

26. Begley M, Jones BV, Hill C, Marchesi JR, Gahan CGM (2008) Functional and comparative metagenomic analysis of bile salt hydrolase activity in the human gut microbiome. *Proc Natl Acad Sci* 105(36):13580–13585.

27. Maldonado-Valderrama J, Wilde P, MacIerzanka A, MacKie A (2011) The role of bile salts in digestion. *Adv Colloid Interface Sci* 165:36–46.

28. Keitel V, Kubitz R, Häussinger D (2008) Endocrine and paracrine role of bile acids. *World J Gastroenterol* 14(37):5620–5629.

29. Inagaki T, et al. (2006) Regulation of antibacterial defense in the small intestine by the nuclear bile acid receptor. *Proc Natl Acad Sci* 103(10):3920–3925.

30. Hofmann AF, Eckmann L (2006) How bile acids confer gut mucosal protection against bacteria. *Proc Natl Acad Sci* 103(12):4333–4334.

31. Begley M, Gahan CGM, Hill C (2005) The interaction between bacteria and bile. *FEMS Microbiol Rev* 29(4):625–651.

32. Lambert JM, Siezen RJ, de Vos WM, Kleerebezem M (2008) Improved annotation of conjugated bile acid hydrolase superfamily members in Gram-positive bacteria. *Microbiology* 154(8):2492–2500.

33. Panigrahi P, Sule M, Sharma R, Ramasamy S, Suresh CG (2014) An improved method for specificity annotation shows a distinct evolutionary divergence among the microbial enzymes of the cholylglycine hydrolase family. *Microbiology* 160(Pt 6):1162–1174.

34. Dussurget O, et al. (2002) Listeria monocytogenes bile salt hydrolase is a PrfA-regulated virulence factor involved in the intestinal and hepatic phases of listeriosis. *Mol Microbiol* 45(4):1095–106.

35. Delpino MV, et al. (2007) A Bile Salt Hydrolase of Brucella abortus Contributes to the Establishment of a Successful Infection through the Oral Route in Mice. *Infect Immun* 75(1):299–305.

36. Avinash VS, Pundle AV, Ramasamy S, Suresh CG (2016) Penicillin acylases revisited: Importance beyond their industrial utility. *Crit Rev Biotechnol* 36(2):303–316.

37. Arroyo M, de la Mata I, Acebal C, Castillón MP (2003) Biotechnological applications of penicillin acylases: state-of-the-art. *Appl Microbiol Biotechnol* 60(5):507–514.

38. Parmar A, Kumar H, Marwaha SS, Kennedy JF (2000) Advances in enzymatic transformation of penicillins to 6-aminopenicillanic acid (6-APA). *Biotechnol Adv* 18(4):289–301.

39. Sio CF, Quax WJ (2004) Improved β-lactam acylases and their use as industrial biocatalysts. *Curr Opin Biotechnol* 15(4):349–355.

40. Valle F, Balbás P, Merino E, Bollvar F (1991) The role of penicillin amidases in nature and industry. *Trends Biochem Sci* 16:36–40.

41. Cole M, Sutherland R (1966) The Role of Penicillin Acylase in the Resistance of Gram-Negative Bacteria to Penicillins. *J Gen Microbiol* 42(3):345–356.

42. Avinash VS, Ramasamy S, Suresh CG, Pundle A (2015) Penicillin V acylase from Pectobacterium atrosepticum exhibits high specific activity and unique kinetics. *Int J Biol Macromol* 79:1–7.

43. Galán B, García JL, Prieto MA (2004) The PaaX Repressor, a Link between Penicillin G Acylase and the Phenylacetyl-Coenzyme A Catabolon of Escherichia coli W. *J Bacteriol* 186(7):2215–2220.

44. Wahjudi M, et al. (2011) PA0305 of Pseudomonas aeruginosa is a quorum quenching acylhomoserine lactone acylase belonging to the Ntn hydrolase superfamily. *Microbiology* 157:2042–2055.

45. Sunder AV, et al. (2017) Penicillin V acylases from gram-negative bacteria degrade N-acylhomoserine lactones and attenuate virulence in Pseudomonas aeruginosa. *Appl Microbiol Biotechnol* 101(6):2383–2395.

46. Davies J (2006) Are antibiotics naturally antibiotics? *J Ind Microbiol Biotechnol* 33(7):496–499.

47. Suresh CG, et al. (1999) Penicillin V acylase crystal structure reveals new Ntn-hydrolase family members. *Nat Struct Biol* 6(5):414–416.

48. Ben-Bassat A, et al. (1987) Processing of the Initiation Methionine from Proteins: Properties of the Escherichia coli Methionine Aminopeptidase and Its Gene Structure. *J Bacteriol* 169(2):751–757.

49. Isupov MN, et al. (1996) Substrate binding is required for assembly of the active conformation of the catalytic site in Ntn amidotransferases: evidence from the 1.8 A crystal structure of the glutaminase domain of glucosamine 6-phosphate synthase. *Struct Lond Engl 1993* 4(7):801–810.

50. Kim JH, Krahn JM, Tomchick DR, Smith JL, Zalkin H (1996) Structure and Function of the Glutamine Phosphoribosylpyrophosphate Amidotransferase Glutamine Site and Communication with the Phosphoribosylpyrophosphate Site. *J Biol Chem* 271(26):15549–15557.

51. Chandra PM, et al. (2005) Cloning, preparation and preliminary crystallographic studies of penicillin V acylase autoproteolytic processing mutants. *Acta Crystallograph Sect F Struct Biol Cryst Commun* 61(1):124–127.

52. Lodola A, et al. (2012) A catalytic mechanism for cysteine N-terminal nucleophile hydrolases, as revealed by free energy simulations. *PloS One* 7(2):e32397.

53. Avinash VS, Panigrahi P, Suresh CG, Pundle AV, Ramasamy S (2013) Structural modelling of substrate binding and inhibition in penicillin V acylase from Pectobacterium atrosepticum. *Biochem Biophys Res Commun* 437(4):538–543.

54. Rutherford ST, Bassler BL (2012) Bacterial Quorum Sensing: Its Role in Virulence and Possibilities for Its Control. *Cold Spring Harb Perspect Med* 2(11):a012427.

55. Li Z, Nair SK (2012) Quorum sensing: How bacteria can coordinate activity and synchronize their response to external signals? *Protein Sci* 21(10):1403–1417.

56. Zhu J, et al. (2002) Quorum-sensing regulators control virulence gene expression in Vibrio cholerae. *Proc Natl Acad Sci* 99(5):3129–3134.

57. Hammer BK, Bassler BL (2003) Quorum sensing controls biofilm formation in Vibrio cholerae. *Mol Microbiol* 50(1):101–104.

58. Duerkop BA, et al. (2009) Quorum-Sensing Control of Antibiotic Synthesis in Burkholderia thailandensis. *J Bacteriol* 191(12):3909–3918.

59. Daniels R, Vanderleyden J, Michiels J (2004) Quorum sensing and swarming migration in bacteria. *FEMS Microbiol Rev* 28(3):261–289.

60. Nealson KH (1977) Autoinduction of bacterial luciferase. Occurrence, mechanism and significance. *Arch Microbiol* 112(1):73–79.

61. Kaplan HB, Greenberg EP (1985) Diffusion of Autoinducer Is Involved in Regulation of the Vibrio fischeri Luminescence System. *J Bacteriol* 163(3):1210–1214.

62. Novick RP, Geisinger E (2008) Quorum Sensing in Staphylococci. *Annu Rev Genet* 42:541–564.

63. Seed PC, Passador L, Iglewski BH (1995) Activation of the Pseudomonas aeruginosa lasI Gene by LasR and the Pseudomonas Autoinducer PAI: an Autoinduction Regulatory Hierarchy. *J Bacteriol* 177(3):654–659.

64. Schaefer AL, Val DL, Hanzelka BL, Cronan JE, Greenberg EP (1996) Generation of cell-to-cell signals in quorum sensing: Acyl homoserine lactone synthase activity of a purified Vibrio fischeri LuxI protein. *Proc Natl Acad Sci U S A* 93(18):9505–9509.

65. Thiel V, Kunze B, Verma P, Wagner-Döbler I, Schulz S (2009) New Structural Variants of Homoserine Lactones in Bacteria. *ChemBioChem* 10(11):1861–1868.

66. Hanzelka BL, Greenberg EP (1995) Evidence that the N-Terminal Region of the Vibrio fischeri LuxR Protein Constitutes an Autoinducer-Binding Domain. *J Bacteriol* 177(3):815–817.

67. Devine JH, Shadel GS, Baldwin TO (1989) Identification of the operator of the lux regulon from the Vibrio fischeri strain ATCC7744. *Proc Natl Acad Sci U S A* 86(15):5688–5692.

68. Zhang R, et al. (2002) Structure of a bacterial quorum-sensing transcription factor complexed with pheromone and DNA. *Nature* 417(6892):971–974.

69. Lin Y-H, et al. (2003) Acyl-homoserine lactone acylase from Ralstonia strain XJ12B represents a novel and potent class of quorum-quenching enzymes. *Mol Microbiol* 47(3):849–860.

70. Koch G, Nadal-Jimenez P, Cool RH, Quax WJ (2014) Deinococcus radiodurans can interfere with quorum sensing by producing an AHL-acylase and an AHL-lactonase. *FEMS Microbiol Lett* 356(1):62–70.

71. Leadbetter JR, Greenberg EP (2000) Metabolism of Acyl-Homoserine Lactone Quorum-Sensing Signals by Variovorax paradoxus. *J Bacteriol* 182(24):6921–6926.

72. Yates EA, et al. (2002) N-Acylhomoserine Lactones Undergo Lactonolysis in a pH-, Temperature-, and Acyl Chain Length-Dependent Manner during Growth of Yersinia pseudotuberculosis and Pseudomonas aeruginosa. *Infect Immun* 70(10):5635–5646.

73. Tait K, et al. (2009) Turnover of quorum sensing signal molecules modulates cross-kingdom signalling. *Environ Microbiol* 11(7):1792–1802.

74. Uroz S, Dessaux Y, Oger P (2009) Quorum Sensing and Quorum Quenching: The Yin and Yang of Bacterial Communication. *ChemBioChem* 10(2):205–216.

75. Krzeslak J, Quax WJ, Wahjudi M (2007) Quorum-Quenching Acylases in Pseudomonas aeruginosa. *Pseudomonas* (Springer Netherlands, Dordrecht), pp 429–449.

76. Hammer ND, Skaar EP (2011) Molecular Mechanisms of Staphylococcus aureus Iron Acquisition. *Annu Rev Microbiol* 65(1):129–147.

77. Hider RC, Kong X (2010) Chemistry and biology of siderophores. *Nat Prod Rep* 27(5):637–657.

78. Beasley FC, Marolda CL, Cheung J, Buac S, Heinrichs DE (2011) Staphylococcus aureus transporters Hts, Sir, and Sst capture iron liberated from human transferrin by staphyloferrin A, staphyloferrin B, and catecholamine stress hormones, respectively, and contribute to virulence. *Infect Immun* 79(6):2345–2355.

79. Xiong A, Singh VK, Cabrera G, Jayaswal RK (2000) Molecular characterization of the ferric-uptake regulator. Fur, from Staphylococcus aureus. *Microbiology* 146(3):659–668.

80. Miethke M, Marahiel MA (2007) Siderophore-Based Iron Acquisition and Pathogen Control. *Microbiol Mol Biol Rev* 71(3):413–451.

81. Hannauer M, Barda Y, Mislin GLA, Shanzer A, Schalk IJ (2010) The ferrichrome uptake pathway in Pseudomonas aeruginosa involves an iron release mechanism with acylation of the siderophore and recycling of the modified desferrichrome. *J Bacteriol* 192(5):1212–1220.

82. Hannauer M, Arifin AJ, Heinrichs DE (2015) Involvement of reductases IruO and NtrA in iron acquisition by Staphylococcus aureus. *Mol Microbiol* 96(6):1192–1210.

83. Kobylarz MJ, Heieis GA, Loutet SA, Murphy MEP (2017) Iron Uptake Oxidoreductase (IruO) Uses a Flavin Adenine Dinucleotide Semiquinone Intermediate for Iron-Siderophore Reduction. *ACS Chem Biol* 12(7):1778–1786.

84. Mäder U, et al. (2016) Staphylococcus aureus Transcriptome Architecture: From Laboratory to Infection-Mimicking Conditions. *PLoS Genet* 12(4):1–32.

85. Hames C, Halbedel S, Schilling O, Stülke J (2005) Multiple-mutation reaction: a method for simultaneous introduction of multiple mutations into the glpK gene of Mycoplasma pneumoniae. *Appl Environ Microbiol* 71(7):4097–4100.

86. Bae T, Schneewind O (2006) Allelic replacement in Staphylococcus aureus with inducible counter-selection. *Plasmid* 55(1):58–63.

87. Coleman JP, Hudson LL (1995) Cloning and characterization of a conjugated bile acid hydrolase gene from Clostridium perfringens. *Appl Environ Microbiol* 61(7):2514–2520.

88. Kabsch W (2010) XDS. *Acta Crystallogr D Biol Crystallogr* 66(2):125–132.

89. Adams PD, et al. (2010) PHENIX: a comprehensive Python-based system for macromolecular structure solution. *Acta Crystallogr D Biol Crystallogr* 66(2):213–221.

90. Bunkóczi G, Read RJ (2011) Improvement of molecular-replacement models with Sculptor. *Acta Crystallogr D Biol Crystallogr* 67(4):303–312.

91. McCoy AJ, et al. (2007) Phaser crystallographic software. *J Appl Crystallogr* 40(4):658–674.

92. Emsley P, Lohkamp B, Scott WG, Cowtan K (2010) Features and development of Coot. *Acta Crystallogr D Biol Crystallogr* 66(Pt 4):486–501.

93. Krissinel E, Henrick K (2005) Multiple Alignment of Protein Structures in Three Dimensions. *Computational Life Sciences*, Lecture Notes in Computer Science., eds R. Berthold M, Glen RC, Diederichs K, Kohlbacher O, Fischer I (Springer Berlin Heidelberg), pp 67–78.

94. Trott O, Olson AJ (2010) AutoDock Vina: improving the speed and accuracy of docking with a new scoring function, efficient optimization and multithreading. *J Comput Chem* 31(2):455–461.

95. Seeliger D, de Groot BL (2010) Ligand docking and binding site analysis with PyMOL and Autodock/Vina. *J Comput Aided Mol Des* 24(5):417–422.

96. Shewale JG, Kumar KK, Ambekar GR (1987) Evaluation of determination of 6-aminopenicillanic acid by p-dimethyl aminobenzaldedyde. *Biotechnol Tech* 1(1):69–72.

97. Stookey LL (1970) Ferrozine---a new spectrophotometric reagent for iron. *Anal Chem* 42(7):779–781.

98. Cotton JL, Tao J, Balibar CJ (2009) Identification and characterization of the Staphylococcus aureus gene cluster coding for staphyloferrin A. *Biochemistry* 48(5):1025–1035.

99. Qazi S, et al. (2006) Lactones Antagonize Virulence Gene Expression and Quorum Sensing in Staphylococcus aureus. *Infect Immun* 74(2):910–919.

100. Loomis LD, Raymond KN (1991) Solution equilibria of enterobactin and metal-enterobactin complexes. *Inorg Chem* 30(5):906–911.

101. Lin H, Fischbach MA, Liu DR, Walsh CT (2005) In Vitro Characterization of Salmochelin and Enterobactin Trilactone Hydrolases IroD, IroE, and Fes. *J Am Chem Soc* 127(31):11075–11084.

102. Zhu M, Valdebenito M, Winkelmann G, Hantke K (2005) Functions of the siderophore esterases IroD and IroE in iron-salmochelin utilization. *Microbiology* 151(7):2363–2372.

103. Koch G, et al. (2014) Reducing virulence of the human pathogen Burkholderia by altering the substrate specificity of the quorum-quenching acylase PvdQ. *PNAS* 111(4):1568–1573.

104. Avinash VS, et al. (2016) Structural analysis of a penicillin V acylase from Pectobacterium atrosepticum confirms the importance of two Trp residues for activity and specificity. *J Struct Biol* 193(2):85–94.

105. Rathinaswamy P, et al. (2005) Cloning, purification, crystallization and preliminary structural studies of penicillin V acylase from Bacillus subtilis. *Acta Crystallograph Sect F Struct Biol Cryst Commun* 61(7):680–683.

106. Rathinaswamy P, et al. (2012) Purification and characterization of YxeI, a penicillin acylase from Bacillus subtilis. *Int J Biol Macromol* 50(1):25–30.

107. Philem PD, Sonalkar VV, Dharne MS, Prabhune AA (2016) Purification and partial characterization of novel penicillin V acylase from Acinetobacter sp. AP24 isolated from Loktak Lake, an Indo-Burma biodiversity hotspot. *Prep Biochem Biotechnol* 46(5):524–530.

108. Orazi G, O'Toole GA (2017) Pseudomonas aeruginosa Alters Staphylococcus aureus Sensitivity to Vancomycin in a Biofilm Model of Cystic Fibrosis Infection. *mBio* 8(4):e00873-17.

109. Gotschlich A, et al. (2001) Synthesis of Multiple N-Acylhomoserine Lactones is Wide-spread Among the Members of the Burkholderia cepacia Complex. *Syst Appl Microbiol* 24(1):1–14.

110. Saroj SD, Holmer L, Berengueras JM, Jonsson AB (2017) Inhibitory role of acyl homoserine lactones in hemolytic activity and viability of Streptococcus pyogenes M6 S165. *Sci Rep* 7:44902.

111. Kaufmann GF, et al. (2005) Revisiting quorum sensing: Discovery of additional chemical and biological functions for 3-oxo-N-acylhomoserine lactones. *Proc Natl Acad Sci* 102(2):309–314.

112. Lowery CA, et al. (2009) Defining the mode of action of tetramic acid antibacterials derived from Pseudomonas aeruginosa quorum sensing signals. *J Am Chem Soc* 131(40):14473–14479.

113. Gandhi NM, Nazareth J, Divekar PV, Kohl H, Souza NJD (1973) Magnesidin, a Novel Magnesium-Containing Antibiotic. *J Antibiot (Tokyo)* 26(12):797–798.

114. Olsson A, Hagstrom T, Nilsson B, Uhlén M, Gatenbeck S (1985) Molecular cloning of Bacillus sphaericus penicillin V amidase gene and its expression in Escherichia coli and Bacillus subtilis. *Appl Environ Microbiol* 49(5):1084–1089.

115. Zhang D, Koreishi M, Imanaka H, Imamura K, Nakanishi K (2007) Cloning and characterization of penicillin V acylase from Streptomyces mobaraensis. *J Biotechnol* 128(4):788–800.

116. Cheynier V (2012) Phenolic compounds: from plants to foods. *Phytochem Rev* 11(2–3):153–177.

117. Balasundram N, Sundram K, Samman S (2006) Phenolic compounds in plants and agri-industrial by-products: Antioxidant activity, occurrence, and potential uses. *Food Chem* 99(1):191–203.